

The University of Maine

DigitalCommons@UMaine

---

Electronic Theses and Dissertations

Fogler Library

---

Summer 8-16-2024

## Flexural Behavior of Scaled-Down Cross-Laminated Timber Beams Under Short- and Long-Term Loadings: Experimental & Numerical Investigations

Maitham Alabbad  
maitham.alabbad@maine.edu

Follow this and additional works at: <https://digitalcommons.library.umaine.edu/etd>



Part of the [Civil Engineering Commons](#), [Computational Engineering Commons](#), [Mechanical Engineering Commons](#), [Structural Engineering Commons](#), and the [Structural Materials Commons](#)

---

### Recommended Citation

Alabbad, Maitham, "Flexural Behavior of Scaled-Down Cross-Laminated Timber Beams Under Short- and Long-Term Loadings: Experimental & Numerical Investigations" (2024). *Electronic Theses and Dissertations*. 4045.

<https://digitalcommons.library.umaine.edu/etd/4045>

This Open-Access Thesis is brought to you for free and open access by DigitalCommons@UMaine. It has been accepted for inclusion in Electronic Theses and Dissertations by an authorized administrator of DigitalCommons@UMaine. For more information, please contact [um.library.technical.services@maine.edu](mailto:um.library.technical.services@maine.edu).

**FLEXURAL BEHAVIOR OF SCALED-DOWN CROSS-LAMINATED TIMBER  
BEAMS UNDER SHORT- AND LONG-TERM LOADINGS:  
EXPERIMENTAL & NUMERICAL INVESTIGATIONS**

By

Maitham Alabbad

B.S. University of Maine, 2017

M.S. University of Maine, 2020

A THESIS

Submitted in Partial Fulfillment of the

Requirements for the Degree of

Master of Science

(in Forest Resources)

The Graduate School

The University of Maine

August 2024

Advisory Committee:

Ling Li, Assistant Professor of Sustainable Bioenergy Systems, Advisor

Zhiyong Chen, Senior Scientist at FPInnovations, Vancouver, BC, CA, Co-Advisor

Stephen Shaler, Professor of Sustainable Material

© 2024 Maitham Alabbad

All Rights Reserved

## **UNIVERSITY OF MAINE GRADUATE SCHOOL LAND ACKNOWLEDGMENT**

The University of Maine recognizes that it is located on Marsh Island in the homeland of Penobscot people, where issues of water and territorial rights, and encroachment upon sacred sites, are ongoing. Penobscot homeland is connected to the other Wabanaki Tribal Nations— the Passamaquoddy, Maliseet, and Micmac—through kinship, alliances, and diplomacy. The University also recognizes that the Penobscot Nation and the other Wabanaki Tribal Nations are distinct, sovereign, legal and political entities with their own powers of self-governance and self-determination.

**FLEXURAL BEHAVIOR OF SCALED-DOWN CROSS-LAMINATED TIMBER  
BEAMS UNDER SHORT- AND LONG-TERM LOADINGS:  
EXPERIMENTAL & NUMERICAL INVESTIGATIONS**

By Maitham Alabbad

Thesis Advisor: Dr. Ling Li

An Abstract of the Thesis Presented  
In Partial Fulfillment of the Requirements for the  
Master of Science  
(in Forest Resources)  
August 2024

Cross-laminated timber (CLT), a product in the mass timber family, is an innovative engineered wood product that enables the construction of mid- and high-rise timber buildings. CLT has been used extensively in timber construction. A typical use of CLT panels is in the construction of walls, floors, and roofs which can carry a continuous load. This load can impact the long-term performance of the CLT structure and must be considered in the design phase.

The primary goal of this research was to better understand the long-term creep behavior of CLT beams and contribute to the development of numerical approaches. The creep performance of CLT beams was assessed under elevated relative humidities using computational simulation and validated against experimental investigation. This study consists of two parts. In the first part, the flexural response of CLT beams was assessed. Material characterization experiments were conducted on spruce to provide the necessary material data for the numerical models. Flexural tests of CLT beams were performed to determine the modulus of elasticity (MOE) and modulus of rupture (MOR) of the CLT beams. In addition to the experimental work, a computational model was developed to predict the flexural response of CLT beam. The 3D Hashin failure criterion was adopted to predict the intralaminar failure of the CLT beam. The mean experimental and numerical values of MOE of the CLT beam were 9.14

GPa and 8.69 GPa, respectively with a difference of 5.10 %. In terms of the MOR, the mean experimental value and numerical value were 39.16 MPa and 40.11 MPa, respectively with a difference of less than 3 %.

The second part of this study was focused on the assessment of creep performance of the CLT beam. A finite element creep model was developed to predict the interaction between the stress and moisture content change in the CLT beam simultaneously loaded under a constant dead load and subject to an elevated relative humidity condition, 30%, 60%, and 90%. ABAQUS user-defined UMAT and DFLUX subroutines were used to evaluate the material behavior and the elevated relative humidity loadings, respectively. The numerical model showed a well prediction of the moisture content distribution in the CLT model. Also, the numerical deflection result had shown a good agreement when compared to the experimental creep deflection. The results of this study showed that the current computational model can be used to predict the long-term creep behavior of such beams, and it can easily be adapted to account for different timber and geometry once the appropriate material properties are available.

## DEDICATION

----- *To family* -----

## ACKNOWLEDGEMENTS

I am grateful to all the people who supported and assisted me throughout this journey. I want to thank my family, especially my parents and my wife for their support, encouragement, and motivation throughout my challenging time.

I would like to thank my advisor Dr. Ling Li for her support, feedback and guidance to make this accomplishment happen. Also, I would like to acknowledge my committee members, Dr. Zhiyong Chen and Dr. Stephen Shaler, for their time and effort in reading and evaluating my work.

I would also like to extend my appreciation to all the people who provided me their assistance in my experimental work, including Chris London (SFR), Benjamin Herzog (ASCC), Jake Snow (ASCC), Andy Brown (Facilities management, UMaine), Christopher Urquhart (ASCC), Sandesh Thapa, and Yu Zhang.

Lastly, I would like to acknowledge Maine Agricultural and Forest Experiment Station (MAFES) for providing the financial support for this project.

## TABLE OF CONTENTS

DEDICATION .....	iv
ACKNOWLEDGEMENTS.....	v
LIST OF TABLES .....	ix
LIST OF FIGURES .....	x
CHAPTER 1: Flexural Response of Thin Cross-Laminated Timber Beams: Experimental and Numerical Investigations .....	1
1.1 Introduction.....	1
1.2 Materials .....	3
1.2.1 Lumber Preparation .....	4
1.2.2 Primer and Adhesive .....	4
1.2.3 CLT Fabrication .....	5
1.3 Experimental Methods.....	7
1.3.1 Specimen Preparation .....	7
1.3.2 Static Bending Testing .....	7
1.3.3 CLT Flexural Testing .....	9
1.4 Numerical Approach.....	11
1.4.1 Elastic Properties of Clear Spruce Wood.....	11
1.4.2 Model Development.....	13
1.4.3 Contact Definition.....	13
1.4.4 Boundary Conditions .....	14
1.4.5 Intralaminar Damage Evaluation .....	14

1.5 Flexural Modulus of CLT Using Classical Laminate Theory .....	17
1.6 Results and Discussion .....	18
1.6.1 Experimental Results .....	18
1.6.1.1 Static Bending Tests Results .....	18
1.6.1.2 CLT Flexural Tests Results .....	20
1.6.2 Numerical Results .....	22
1.6.2.1 Elastic Properties Computations .....	22
1.6.2.2 Flexural Simulation Results .....	23
1.7 Conclusion .....	24
CHAPTER 2: Creep Performance of Scaled-Down Cross-Laminated Timber Beams Under	
Elevated Relative Humidities .....	26
2.1 Introduction.....	26
2.2 Experimental Creep Test Setup.....	31
2.2.1 Materials .....	31
2.2.2 Creep Testing Setup .....	32
2.2.3 Instrumentations.....	33
2.2.4 Environmental Conditions and Loading .....	34
2.3 Numerical Model of Mechano-Sorptive Creep of CLT Beams .....	35
2.3.1 Moisture Diffusion Model .....	36
2.3.2 Strain Components.....	39
2.3.2.1 Elastic Strain Component .....	40

2.3.2.2 Moisture-Induced Strain Component.....	41
2.3.2.3 Thermal Strain Component.....	42
2.3.2.4 Mechano-Sorptive Strain Component.....	42
2.3.2.5 Creep Strain Component.....	43
2.3.3 ABAQUS User-Subroutine UMAT.....	44
2.3.4 Numerical Model Development.....	44
2.3.4.1 Model Geometry.....	44
2.3.4.2 Material Properties.....	45
2.3.4.3 Boundary Conditions.....	47
2.4 Results and Discussion.....	48
2.4.1 Experimental Results.....	48
2.4.2 Numerical Results.....	51
2.4.2.1 Moisture Content Distribution in the FE Model.....	51
2.4.2.2 Creep Deflection of the FE Model.....	54
2.5 Conclusion.....	56
References.....	57
BIOGRAPHY OF THE AUTHOR.....	62

## LIST OF TABLES

### **Chapter 1:**

Table 1. 1 Material strength properties for failure evaluation .....	16
Table 1. 2 Summary of the results for static bending tests of clear wood samples .....	20
Table 1. 3 Summary of the flexural tests results of CLT beams .....	21
Table 1. 4 The elastic properties of Spruce .....	23
Table 1. 5 Summary of the modulus of elasticity and modulus of rupture of the CLT beam.....	24

### **Chapter 2:**

Table 2. 1 Material properties of timber implemented in the numerical model.....	46
Table 2. 2 Comparison between the experimental and numerical deflection .....	55

## LIST OF FIGURES

### **Chapter 1:**

Figure 1. 1 Lumber boards laid side by side for CLT assembly .....	6
Figure 1. 2 CLT assembly before pressing.....	6
Figure 1. 3 CLT billet after pressing .....	7
Figure 1. 4 Static bending tests setup of clear wood.....	8
Figure 1. 5 Sketch of the Third-point test setup.....	10
Figure 1. 6 Third-point test setup of CLT beams .....	10
Figure 1. 7 Principal axes of single piece of lumber used to model the FE CLT beam (source: wood handbook [18]).....	12
Figure 1. 8 The finite element model assembly and boundary conditions application.....	14
Figure 1. 9 Force-displacement curves for the static bending tests of clear wood samples .....	19
Figure 1. 10 Failure modes of CLT specimens .....	22
Figure 1. 11 Numerical flexural force-displacement response of CLT beam compared to experiment.....	23

### **Chapter 2:**

Figure 2. 1 Three phases of creep and the influence of stress loading on the evolution of deformation with time [27] .....	26
Figure 2. 2 Schematic diagram of four-element Burgers model [3, 7, 8] .....	27
Figure 2. 3 Creep deflection of poplar ( <i>Populus euramevicana</i> ) under the RH cycles of 42%- 89%-42% [14].....	29
Figure 2. 4 Sketch of the test configuration and specimen's geometry.....	32
Figure 2. 5 Creep testing frame.....	33

Figure 2. 6 Experimental creep test setup.....	35
Figure 2. 7 Plot of the equilibrium moisture content of wood using different expressions.....	39
Figure 2. 8 The boundary conditions used in the numerical model.....	48
Figure 2. 9 Temperature and relative humidity of the testing chamber .....	49
Figure 2. 10 Experimental creep deflection results of the CLT beams .....	50
Figure 2. 11 Moisture content distribution of the FE CLT after the 30% RH testing period.....	52
Figure 2. 12 Moisture content distribution of the FE CLT after the 60% RH testing period .....	53
Figure 2. 13 Moisture content distribution of the FE CLT after the 90% RH testing period .....	53
Figure 2. 14 Plot of moisture content of the FE CLT model from three different locations.....	54
Figure 2. 15 The numerical creep deflection of the CLT beam compared to the mean experimental result.....	55

# **CHAPTER 1: Flexural Response of Thin Cross-Laminated Timber Beams: Experimental and Numerical Investigations**

## **1.1 Introduction**

Cross-laminated timber (CLT) has become an increasingly popular and competitive in mid and high rise buildings in Europe, it was introduced in Austria and Germany in the mid-1990s. CLT has gained a lot of interest in North America with the establishment of several CLT plants in Canada and the United States due to its good structural properties and low environmental impact (e.g., low embodied carbon). CLT panels are commonly used in walls, floors, and roofs constructions. CLT panels consist of at least three layers of lumber stacked crosswise and glued together and are typically fabricated from an odd number of layers (3, 5, 7, or more) of solid-sawn lumber placed in alternating 90-degree directions [1]. Due to this configuration, CLT is formed in a plate-like shape and can withstand a load both in-plane and out-of-plane. Compared to typical building materials, concrete and steel, CLT is valued for its high strength-to-bending ratios and capacity for quick and efficient assembly of strong structures [2]. Besides the conventional CLT panels made of dimension lumber (i.e., 2x4, 2x6, 2x8 softwood lumber) and hybrid CLT panels consisting of dimension lumber and wood composites (plywood, laminated strand lumber), a new type of thin CLT panel fabricated using thin boards with a thickness less than 25 mm (~1 inch) has been found in the market [28]. It can be used as interior paneling, a single-family house wall component, and more.

When using CLT panels in various applications, the strength and stiffness performance needs to be assessed. Besides the experimental testing methods, a widely used approach to evaluate wood materials is through the finite element (FE) method. Numerical simulation is a powerful tool and has been shown to be capable of predicting the structural response of a material. This tool has an effect on complex and expensive experimental work which can be reduced using numerical

simulation. Numerical simulations of CLT can be performed using 1D, 2D, or 3D models. Thiel and Schickhofer [3] used CLTdesigner software to develop a 1D plate design of CLT under load out of plane, their work aims to provide verification of bending and shear stresses for the ultimate limit state for persistent, transient, and accidental design situations, as well as for the verification of deformation and vibration. The FE 2D models are fast and give reasonable outputs, they are often evaluated using Kirchhoff or Mindlin-Reinser plate theory ( [4] and [5]). The 1D and 2D models are good to get the general structural response but do not provide a lot of details such as stress distribution and failure mechanism when the study evaluating damage of the structure. Also, higher order theories which can result in an accurate structural response have been used to evaluate CLT panel ( [6] and [7]). However, the higher order theories are not commonly implemented in commercial FE software, and some of these software require additional or external subroutines to implement higher order theories or evaluation criteria.

He et al. [8] investigated the bending and compressive properties of CLT made from Canadian hemlock using numerical simulations and validated their FE results against experiment. The comparison between the experimental and numerical results illustrated that the numerical results correlate well with the experiment. Chen et al. [9] investigated the flexural performance of box-based CLT system with different plate layups/angles. Their study was carried out experimentally and using the FE software package ANSYS. The CLT models in the study are capable of providing a prediction of the combined structure system under out-of-plane loading. Gharib et al. [10] presented an orthotropic 3D constitutive model which was developed for fibrous materials, and it was utilized for the non-linear analysis of timber members with arbitrary orientation of the grain direction. Different modes of failure and their representative failure criteria are implemented in ABAQUS to evaluate failure. Brank et al. [11] presented a procedure of optimizing and modeling ribbed CLT plates. A numerical model for a complete failure analysis was considered to estimate

the limit load, limit ductility and failure mechanism of a ribbed CLT plate. The studied model was based on the Hashin failure criteria, and it was approved that the Hashin failure criteria is capable of predicting the failure mechanism of the CLT. Gecys et al. [12] performed numerical simulations to study the bending behavior of a new type of timber mounting connection. In Gecys study, they adopted Hill criterion to evaluate failure, however, Hill criterion does not account for the difference between tension and compression or the various failure modes. Wang et al. [13] carried out experimental and numerical investigations on the fire behavior of loaded cross-laminated timber panels. In their study, a 3D finite element model was developed and the Hashin criterion and cohesive elements were adopted to predict the failure of wood and adhesive. The FE model was validated with experimental results and was found to have the ability to simulate the fire behavior of loaded cross-laminated timber panels in acceptable accuracy.

Thus, this work aimed to develop a 3D FE model of CLT beams using ABAQUS [14]. The FE model was developed to evaluate the flexural response and effectively predict the modulus of elasticity, modulus of rupture, and failure mechanism of CLT beams. The effectiveness of the 3D FE model was validated by testing 3-ply CLT beam samples made of thin Spruce lumber pieces.

## **1.2 Materials**

The lumber used in this study was Spruce (*Picea*). Spruce lumber was purchased from a local supplier in Old Town, Maine. The lumber was 38 mm (thickness) x 140 mm (width) x 2438 mm (length) (2" x 6" x 96"). The lumber was kiln dried and heat treated (KD-HT), and the grade was No. 2 and better. The lumber was stored in a room where the relative humidity was maintained to be around  $60 \pm 5\%$  and temperature was around  $23 \pm 3\text{ }^{\circ}\text{C}$ . Loctite® PURbond primer and adhesive was used to fabricate the CLT panel.

The spruce lumber was used to perform static bending tests of small clear wood and to fabricate a 3-ply CLT billet. The CLT specimens were cut from the CLT billet for the flexural and creep tests.

### 1.2.1 Lumber Preparation

Before the fabrication of the CLT billet, the lumber was prepared to meet the desired thickness and width of the CLT. The lumber boards were cut to about 12.5 mm (0.5 in.) thick, and since the thickness of the lumber was reduced, the width of the lumber boards used to assemble the transverse layer of the CLT was reduced proportionally as well. The width of the transverse layer lumber was calculated to be as follows:

$$t_o = 4.5 \text{ in}; t_r = 1.5 \text{ in}; w_o = 5.5 \text{ in} \quad [1.1]$$

Where:

$t_o$  is the original thickness of the CLT billet  
 $t_r$  is the reduced thickness of the CLT billet  
 $w_o$  is the original width of the lumber

$$ratio = \frac{t_o}{t_r} = 3 \quad [1.2]$$

Therefore, the downsized width of the transverse layer ( $w_r$ ) is as follows:

$$w_r = \frac{w_o}{ratio} = 1.83 \text{ in} \quad [1.3]$$

Then, prior to primer and adhesive application and pressing, the lumber boards were planed to the desired thickness and to make the surface of the lumber fresh for the application of the primer and adhesive.

### 1.2.2 Primer and Adhesive

Loctite® PR 3105 PURbond primer and Loctite® PURbond HB X602 adhesive, from Henkel Adhesives, were used as the adhesive system for the CLT fabrication. The primer was applied to each planed lumber surface, and it was spread at a target rate of 20g/m<sup>2</sup> using a hand pump sprayer.

Then the boards were left for 45 minutes after applying the primer to allow it to dry and activate before spreading the adhesive. Then, the adhesive was applied at a spread rate of  $180\text{g/m}^2$ , and it was applied to one of the two faces of the board and hand spread using a putty knife.

### **1.2.3 CLT Fabrication**

The boards of the 3-ply were laid side by side as shown in Figure (1.1) and the amount of adhesive was measured and poured on top and spread. Once the adhesive was applied to the surface of the first layer, the transverse layer boards were laid atop, and adhesive was applied and spread. This process was repeated for the remaining layer. Once the layup was complete, straps were placed around the perimeter and tightened to minimize movement and edge gaps during pressing as shown in Figure (1.2).

Per the Technical Datasheet of the adhesive, an open assembly time (from starting the adhesive application to pressing) of 60 minutes or less was targeted and achieved. Then the panel was pressed at 120 psi for 3 hours in a hydraulic press. Once pressed, the billet was stored in laboratory conditions for at least 48 hours prior to being cut into test specimens. Figure (1.3) shows the CLT billet after pressing.



Figure 1. 1 Lumber boards laid side by side for CLT assembly



Figure 1. 2 CLT assembly before pressing

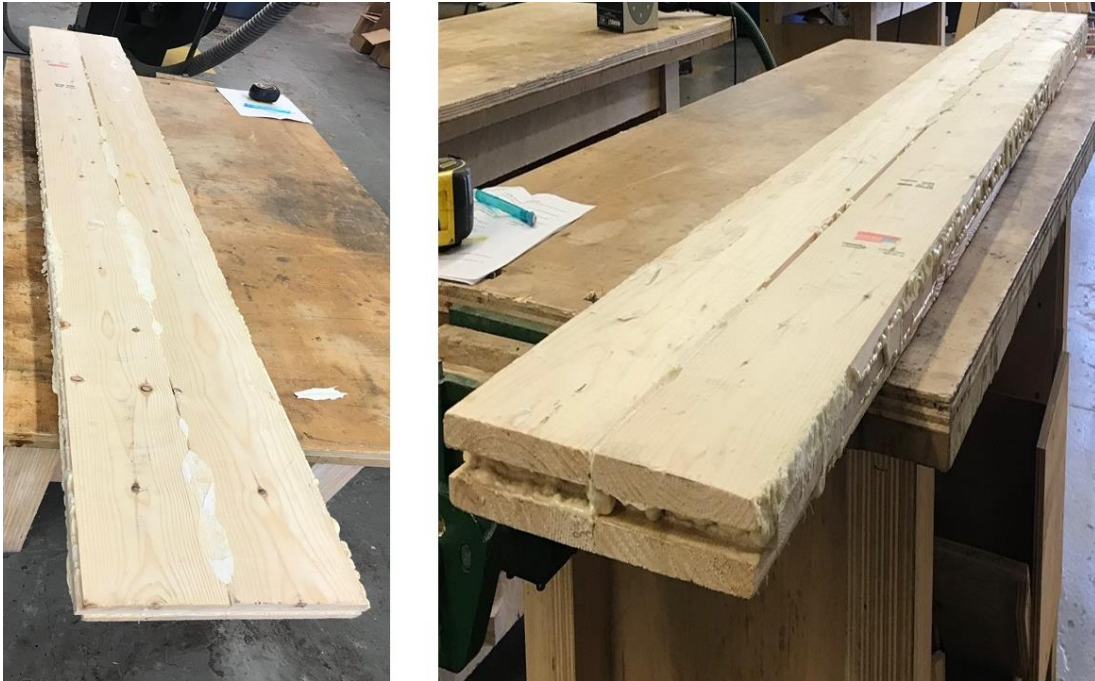


Figure 1. 3 CLT billet after pressing

### **1.3 Experimental Methods**

#### **1.3.1 Specimen Preparation**

Specimens for static bending tests of small clear spruce wood were cut from the lumber boards. For this testing method, nine samples were cut with minimum defects and making sure the grains are straight as much as possible. Also, CLT specimens were cut from the CLT billet to carry out flexural tests. Six CLT specimens were prepared for flexural testing. All specimens were stored in a conditioning chamber for a minimum of a week at  $23 \pm 2$  °C and  $50 \pm 5$  % RH.

#### **1.3.2 Static Bending Testing**

Static bending tests of clear wood specimens were carried out in accordance with ASTM D143-22 [15] using a 100kN Instron testing machine. Nine specimens were tested at an ambient environment, and tests were performed under position control with a speed rate of 2 mm/min (0.079 in/min). The size of the specimens was 25.4 mm x 25.4 mm x 406.4 mm (1 in. x 1 in. x 16 in.) following the secondary method specified in ASTM D143-22. The span length was 355.6 mm

(14 in.) to maintain a span-to-depth ratio of 14. Load and load cell displacement were recorded continuously at 50 Hz by the controller PC and deflection of the specimens was recorded using linear variable inductive transformer (LVIT). It should be noted that the deflection of the specimens was recorded from the center base of the specimen. The static bending tests setup is shown in Figure (1.4).

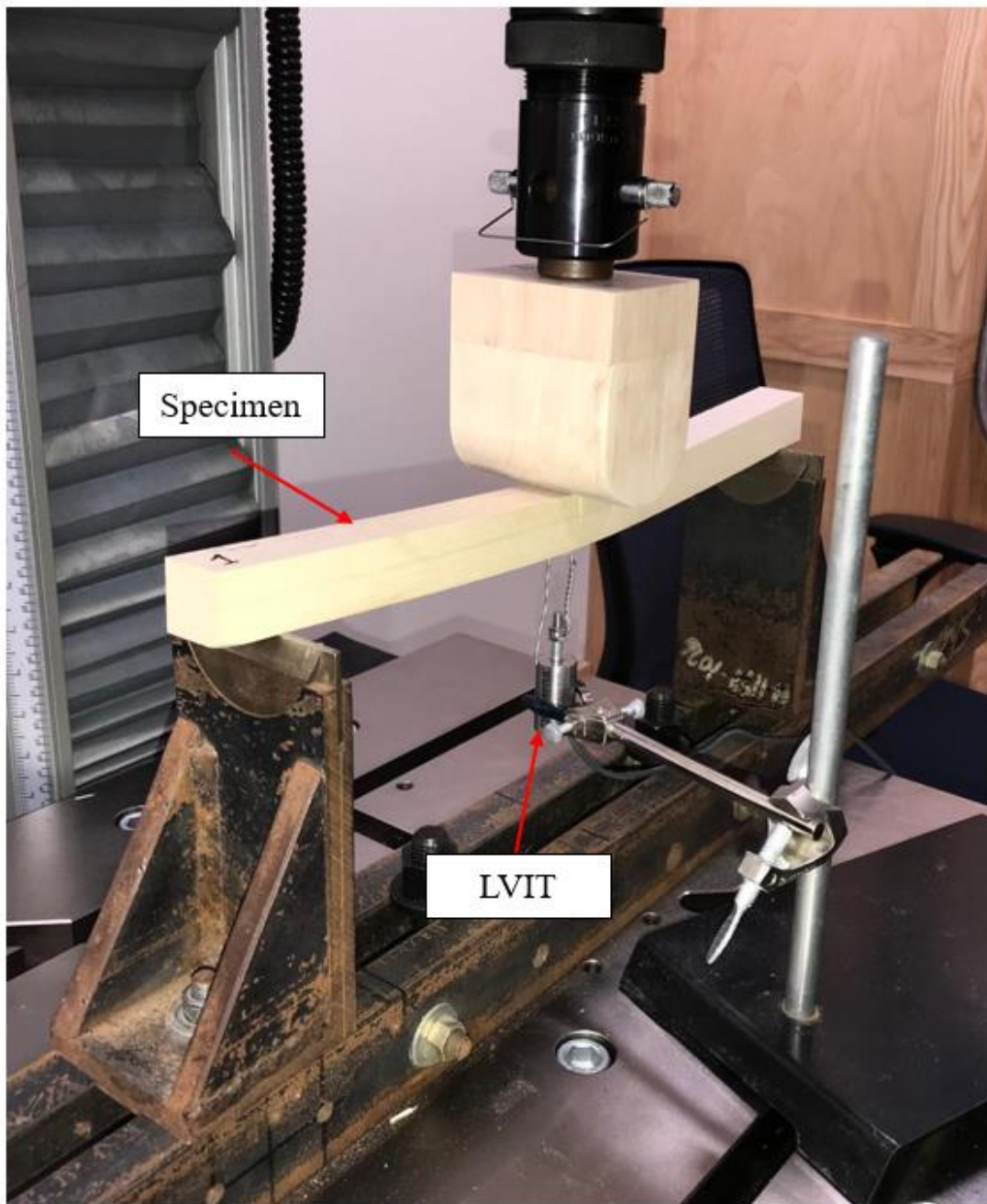


Figure 1. 4 Static bending tests setup of clear wood

The moisture content for each specimen was determined after the test was complete. Also, modulus of elasticity (MOE) and modulus of rupture (MOR) were determined using expression [1.4]. MOE was calculated by using the load and displacement data within the elastic region of the force-displacement curve.

$$MOE = \frac{Pl^3}{4bd^3\Delta} \quad [1.4]$$

$$MOR = \frac{3P_{max}l}{2bd^2}$$

Where:

$P$  is the increment of applied load (N)

$P_{max}$  is the maximum applied load (N)

$l$  is the span length (m)

$b$  is the width (m)

$d$  is the thickness (m)

$\Delta$  is the increment of deflection (m)

### 1.3.3 CLT Flexural Testing

Third point loading flexural tests of CLT specimens were carried out in accordance with ASTM D198-22 [16] using a 25kN Instron testing machine. A sketch of the third point test setup is shown in Figure(1.5). Six CLT specimens were tested at a laboratory condition of  $23 \pm 2$  °C and  $40 \pm 5$  % RH. Tests were performed under position control with a speed rate of 2.54 mm/min (0.1 in/min). The size of the specimens was 63.5 mm x 38.1 mm x 797.4 mm (2.5 in. x 1.5 in. x 31 in.). The span length was 685.8 mm (27 in.) to maintain a span-to-depth ratio of 18. Load and load cell displacement were recorded continuously by the controller PC at 5 Hz for the first three specimens and the other three were tested at a different time and data were recorded at 1 Hz. The deflection of the specimens was recorded from the center base of the specimens using string potentiometer for all specimens as shown in Figure (1.6).

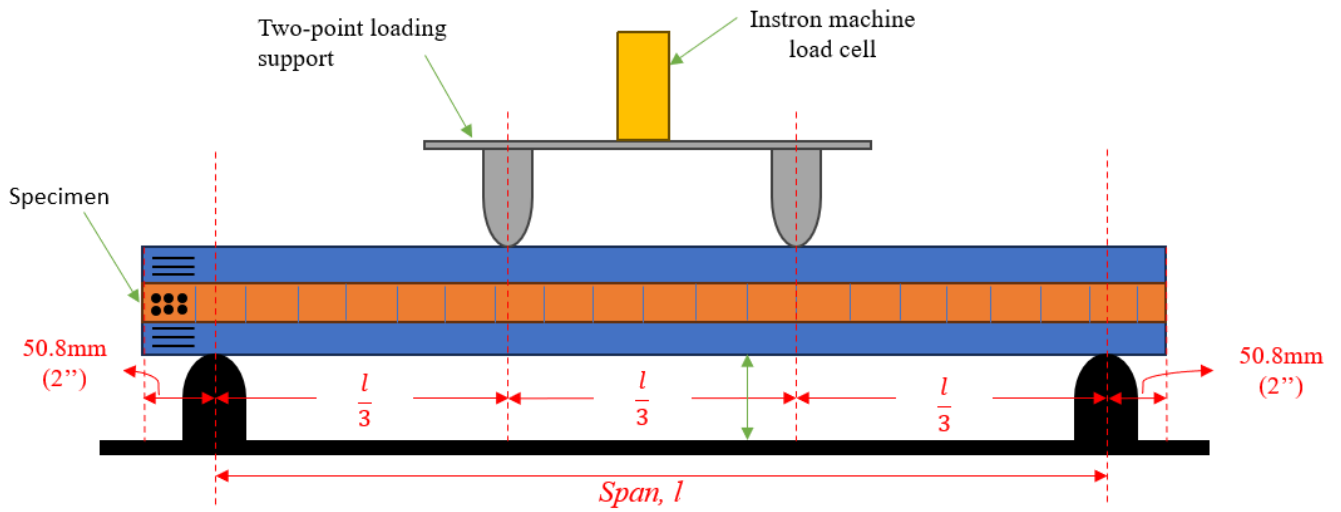


Figure 1. 5 Sketch of the Third-point test setup

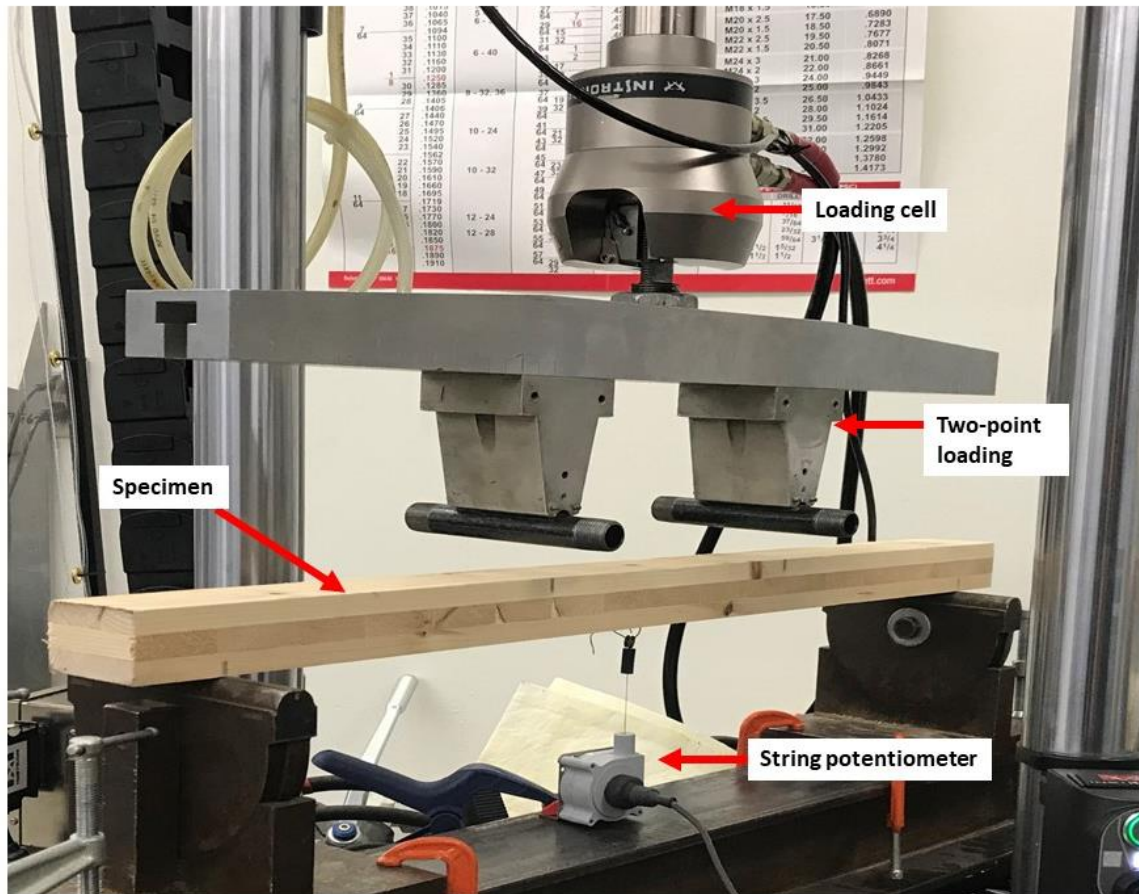


Figure 1. 6 Third-point test setup of CLT beams

The moisture content of the CLT specimens was determined after the test using the oven dry method. Also, the failure location and mode for each specimen were determined, and the modulus of elasticity,  $MOE_{CLT}$ , and modulus of rupture,  $MOR_{CLT}$ , of the CLT were calculated using equation [1.5] for third loading method (ASTM D198-22 [16]). The  $MOE_{CLT}$  was calculated by using the load and displacement data within the elastic region of the force-displacement curve.

$$MOE_{CLT} = \frac{23Pl^3}{108bd^3\Delta} \quad MOR_{CLT} = \frac{P_{max}l}{bd^2} \quad [1.5]$$

Where:

- $P$  is the increment of applied load (N)
- $P_{max}$  is the maximum applied load (N)
- $l$  is the span length (m)
- $b$  is the width (m)
- $d$  is the total thickness of the CLT (m)
- $\Delta$  is the increment of deflection (m)

## 1.4 Numerical Approach

Wood is a complex anisotropic material to work with due to the many factors that can influence its properties. The mechanical properties of wood can be affected by mostly the moisture content, temperature, rate of loading, and other variables. Thus, generating a numerical model of wood material can be challenging. This study was focused on developing a finite element model of CLT to predict its structural response. In this section, the elastic material properties of Spruce were estimated based on the experimental result of the modulus of elasticity in the longitudinal direction (e.g. fiber direction) and some assumptions. Also, a finite element (FE) model was developed to simulate the flexural test and validate its structure response with experiment.

### 1.4.1 Elastic Properties of Clear Spruce Wood

Timber can be regarded as an orthotropic elastic material. In this study, spruce timber was tested experimentally to obtain the modulus of elasticity in the longitudinal (L) direction. Then, the elastic

moduli in the tangential (T) and radial (R) directions as well as the shear moduli in LT, LR, and TR planes were estimated by using the well-known assumption, Bodig and Jayne [17] relationship. Despite the many sources of variation, this relationship suggests that in general the elastic moduli are related according to the following ratios:

$$E_L : E_R : E_T \approx 20 : 1.6 : 1$$

$$G_{LR} : G_{LT} : G_{RT} \approx 10 : 9.4 : 1$$

$$E_L : G_{LR} \approx 14 : 1$$
[1.6]

The Poisson's ratios were calculated using the following expressions [18]:

$$v_{LT} = \frac{E_L}{E_T} v_{TL} ; \quad v_{LR} = \frac{E_L}{E_R} v_{RL} ; \quad v_{TR} = \frac{E_T}{E_R} v_{RT}$$
[1.7]

The subscripts L, R and T refer to the directions of longitudinal, radial, and tangential directions respectively. The elastic material properties are assigned to the FE model according to the principal axes shown in Figure(1.7).

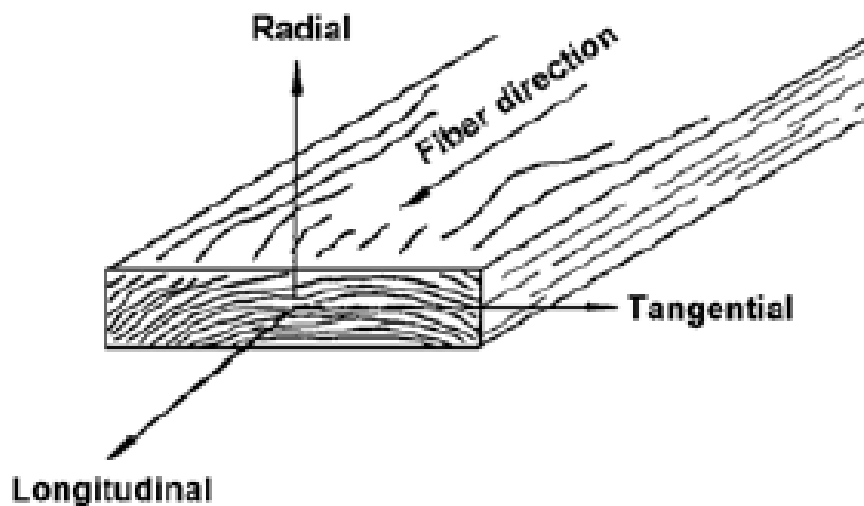


Figure 1. 7 Principal axes of single piece of lumber used to model the FE CLT beam (source: wood handbook [18])

### **1.4.2 Model Development**

A finite element (FE) model was generated in ABAQUS [14] to evaluate the structural response of a 3-ply ( $0^\circ$ ,  $90^\circ$ ,  $0^\circ$ ) CLT beam under flexural loading. The zero degree ( $0^\circ$ ) is the longitudinal direction (i.e., fiber direction, major direction of the CLT panel), while  $90^\circ$  is the transverse direction (i.e., minor direction of the CLT panel). For structural analysis, the FE model was developed with 3D deformable solid elements. The dimensions of CLT beam were 63.5 mm x 38.1 mm x 787.4 mm (width x thickness x length). The material orientation of the plies was defined using the available tool in ABAQUS. A local coordinate system was defined for each ply. Then, each ply was assigned a material orientation based on the local coordinate system of the ply. The CLT beam was meshed using the 3D stress elements. The element type used was the 8-node linear brick C3D8. Fully integrated elements were used with a number of elements of 83,790.

A cylindrical rod was modeled for the third-point flexural test simulation. This beam model was used as a rigid frame to support the specimen and as a loading head. The loading head was used to apply the load without high stress concentration in the specimen. The cylindrical rod was modeled in ABAQUS as a 3D discrete rigid body with a diameter of 50 mm, and it was meshed with linear quadrilateral elements of type R3D4 and linear triangular elements of type R3D3 with a total of 2912 elements.

### **1.4.3 Contact Definition**

The general contact algorithm for ABAQUS analysis was used for flexural test simulations. ABAQUS is a very robust FE analysis package with a proven contact algorithm. This contact method goes through the FE model and defines contact between any two or more solid parts. The contact domain was set to “All with self” with the use of global contact properties. This contact algorithm definition is a necessity in order to prevent penetration between the parts that will be in contact. The contact properties definition was created in the contact property tool in ABAQUS. A

mechanical tangential behavior was defined, assuming that there is a small friction of 0.15 between CLT surfaces and the load head and frame supports. Also, a normal behavior is used for the contact definition, with the ‘Hard’ contact as the pressure-over closure, which means that the friction is applied only when two surfaces are in contact.

#### 1.4.4 Boundary Conditions

The boundary conditions used for the FE CLT model were a representation of the experimental setup used in the flexural test. The frame supports were fixed in all translation and rotation directions. The movement of the load head supports were constraint to a reference point. The load head support was fixed in translation and rotation directions except the z-direction where the load was applied to the reference point using a displacement control method. The applied boundary conditions are shown in Figure (1.8).

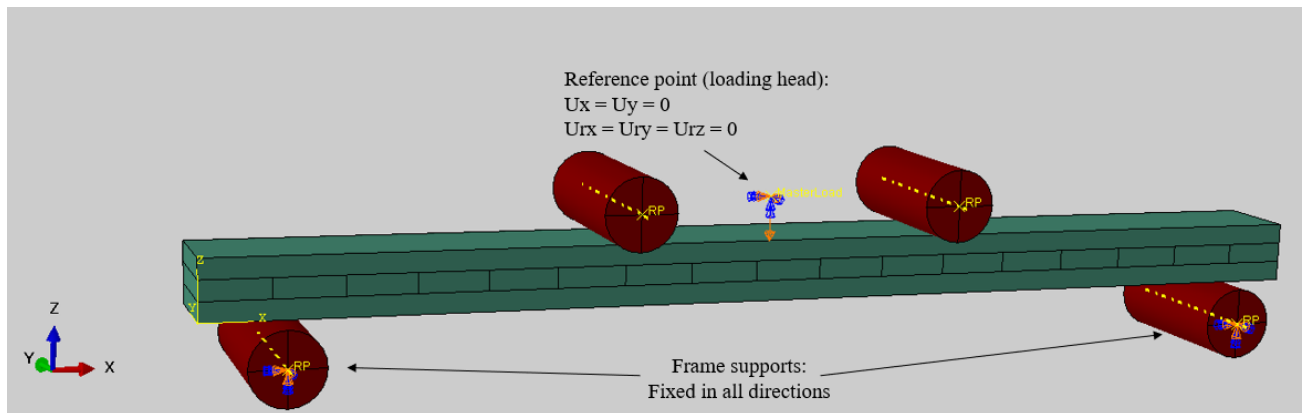


Figure 1. 8 The finite element model assembly and boundary conditions application

#### 1.4.5 Intralaminar Damage Evaluation

The damage evaluation during the flexural test simulation was implemented in ABAQUS using a USDFLD Fortran user subroutine. The subroutine checks for failure initiation at every integration point using the Hashin failure criteria [19] and computes the damage variables using the exponential law. The Hashin failure criteria include four individual failure modes fiber tension and compression modes and transverse tension and compression modes. The four failure modes are

illustrated in Equations (1.8 a-d). The exponential damage evolution law [20] was adopted to calculate the damage variable for each failure mode. The damage evolution law utilizes Equation (1.9) to calculate the damage variable. More details on the intralaminar damage evaluation and implementation in ABAQUS user subroutine were presented in Alabbad et al. [21] and Warren et al. [20].

Fiber tension failure mode ( $\sigma_L > 0$ )

$$F_{ft} = \left(\frac{\sigma_L}{X_T}\right)^2 + \frac{1}{S_{LT}^2}(\sigma_{LT}^2 + \sigma_{LR}^2) \geq 1 \quad [1.8a]$$

Fiber compression failure mode ( $\sigma_L < 0$ )

$$F_{fc} = \left(\frac{\sigma_L}{X_C}\right)^2 \geq 1 \quad [1.8b]$$

Transverse tension failure mode ( $\sigma_T + \sigma_R > 0$ )

$$F_{tt} = \frac{(\sigma_T + \sigma_R)^2}{Y_T^2} + \frac{(\sigma_{TR}^2 - \sigma_T\sigma_R)}{S_{TR}^2} + \frac{1}{S_{LT}^2}(\sigma_{LT}^2 + \sigma_{LR}^2) \geq 1 \quad [1.8c]$$

Transverse compression failure mode ( $\sigma_T + \sigma_R < 0$ )

$$F_{tc} = \frac{1}{Y_C^2} \left[ \left(\frac{Y_C}{2S_{TR}}\right)^2 - 1 \right] (\sigma_T + \sigma_R) + \frac{(\sigma_T + \sigma_R)^2}{4(S_{TR}^2)} + \frac{(\sigma_{TR}^2 - \sigma_T\sigma_R)}{S_{TR}^2} + \frac{1}{S_{LT}^2}(\sigma_{LT}^2 + \sigma_{LR}^2) \geq 1 \quad [1.8d]$$

Where  $\sigma$  are the stress components in the material coordinate system (L is longitudinal, T is transverse, and R is radial),  $X_T$  and  $X_C$  are the axial tensile and compressive strength, respectively.  $Y_T$  and  $Y_C$  are the transverse tensile and compressive strength, respectively and  $S_{LT}$  and  $S_{TR}$  are the axial shear strength and transverse shear strength, respectively. The strength values of spruce

for failure evaluation were obtained from previous studies ( [22], [23], and [24]), and the experimental specimens were reported to be from straight grain, i.e., without knots, cross grains, checks, or cracks. The strength values are listed in Table 1.1.

Table 1. 1 Material strength properties for failure evaluation

Load	Symbol	Strength (MPa)	Source
Tensile strength	$X_T$	61	Rahman et al. [24]
	$Y_T$	3.5	
Compressive strength	$X_C$	40	
	$Y_C$	4.3	Sandhaas et al. [22]
Shear strength	$S_{LT}$	6.9	Rahman et al. [24]
	$S_{TR}$	1.6	Dahl et al. [23]

The exponential damage evolution law expression is as follows:

$$d(F_i) = d_{max} \left[ 1 - \exp \left( -\frac{f_i^m}{m * e} \right) \right] \quad [1.9]$$

Where  $D_{max}$  is the maximum degradation variable,  $F_i$  is the Hashin failure indicator,  $m$  is the material response parameter and  $e$  is the base of the natural logarithm. The material response parameter,  $m$ , as this parameter  $m$  increases, the more brittle the material damage response becomes. Which means that when  $m$  reaches/approaches an infinite value, the exponential damage evolution model becomes an instantaneous damage model. In our study,  $m$  is set to be 200 based on author's the experience and the observation of CLT beam samples' failure behavior.

## 1.5 Flexural Modulus of CLT Using Classical Laminate Theory

Classical laminated theory is a descriptive method for analyzing composite laminates. It can be used to anticipate the structure response of the laminate as a consequence of mechanical loads [25]. However, the classical laminated theory was utilized in this study to predict the MOE of the CLT using the calculated elastic properties. The theoretical prediction of the MOE of the CLT was performed to give a comparison between the theoretical, numerical, and experimental values. This comparison is intended to shed light on the use of theoretical and numerical work.

To predict the theoretical flexural modulus of the CLT,  $MOE_L^{fl}$ , the bending stiffness matrix [D] is computed using the classical laminate theory [25]. The matrix [D] is calculated as follows:

$$[D] = \begin{bmatrix} D_{11} & D_{12} & D_{16} \\ D_{12} & D_{22} & D_{26} \\ D_{16} & D_{26} & D_{66} \end{bmatrix} \quad [1.10]$$

$$[D_{ij}] = \frac{1}{3} \sum_{k=1}^N [\bar{Q}]^k (Z_{k+1}^3 - Z_k^3), \quad i, j = 1, 2, 6 \quad [1.11]$$

Where k is the lamina number, N is the number of the layers, and  $Z_k$  is the coordinate of the k-th lamina.  $[\bar{Q}]$  is the off-axis reduced stiffness matrix, and it is calculated as follows:

$$[\bar{Q}] = \begin{bmatrix} \bar{Q}_{11} & \bar{Q}_{12} & \bar{Q}_{16} \\ \bar{Q}_{12} & \bar{Q}_{22} & \bar{Q}_{26} \\ \bar{Q}_{16} & \bar{Q}_{26} & \bar{Q}_{66} \end{bmatrix} \quad [1.12]$$

where

$$\begin{aligned} \bar{Q}_{11} &= Q_{11}m^4 + 2(Q_{12} + 2Q_{66})m^2n^2 + Q_{22}n^4 \\ \bar{Q}_{12} &= (Q_{11} + Q_{22} - 4Q_{66})m^2n^2 + Q_{12}(m^4 + n^4) \\ \bar{Q}_{16} &= (Q_{11} - Q_{12} - 2Q_{66})m^3n + (Q_{12} - Q_{22} + 2Q_{66})n^3m \\ \bar{Q}_{22} &= Q_{11}n^4 + 2(Q_{12} + 2Q_{66})m^2n^2 + Q_{22}m^4 \\ \bar{Q}_{26} &= (Q_{11} - Q_{12} - 2Q_{66})n^3m + (Q_{12} - Q_{22} + 2Q_{66})m^3n \end{aligned} \quad [1.13]$$

$$\bar{Q}_{66} = (Q_{11} + Q_{22} - 2Q_{12} - 2Q_{66})m^2n^2 + Q_{66}(m^4 + n^4)$$

$$m = \cos\theta \quad , \quad n = \sin\theta$$

$$Q_{11} = \frac{E_L}{1 - \nu_{LT}\nu_{TL}}$$

$$Q_{12} = \frac{\nu_{LT}E_T}{1 - \nu_{LT}\nu_{TL}}$$

$$Q_{22} = \frac{E_T}{1 - \nu_{LT}\nu_{TL}}$$

$$Q_{66} = G_{LT}$$

Therefore, the theoretical flexural modulus of the CLT,  $MOE_L^{fl}$ , is computed using the following equation:

$$MOE_L^{fl} = \frac{12(D_{11}D_{22} - D_{12}^2)}{D_{22}H^3} \quad [1.14]$$

where H is the total thickness of the laminate.

## 1.6 Results and Discussion

### 1.6.1 Experimental Results

#### 1.6.1.1 Static Bending Tests Results

The force-displacement response of the clear spruce specimens is shown in Figure (1.9). The MOE in the longitudinal direction was calculated for each specimen, a summary of the results is presented in Table 1.2. The mean and standard deviation (SD) values of MOE were  $10.91 \pm 0.73$  GPa with coefficient of variation (COV) of 6.67%. The average MOE was then used to estimate the other elastic properties using Equation (1.6). In addition, the mean and SD of MOR were  $70.00 \pm 6.48$  MPa with a COV of 9.25%. The failure type was observed to be a combination of simple tension and cross-grain tension as illustrated in ASTM D143-22 [15].

The moisture content (MC) was calculated for each specimen using the oven dry method, a summary of the results is presented in Table 1.2. Once the test was done, a small section approximately 25 mm (1 in.) in length was cut from each specimen near the failure point for moisture content calculation. The mean and SD of MC were  $9.02 \pm 0.28$  % with a COV of 3.14%.

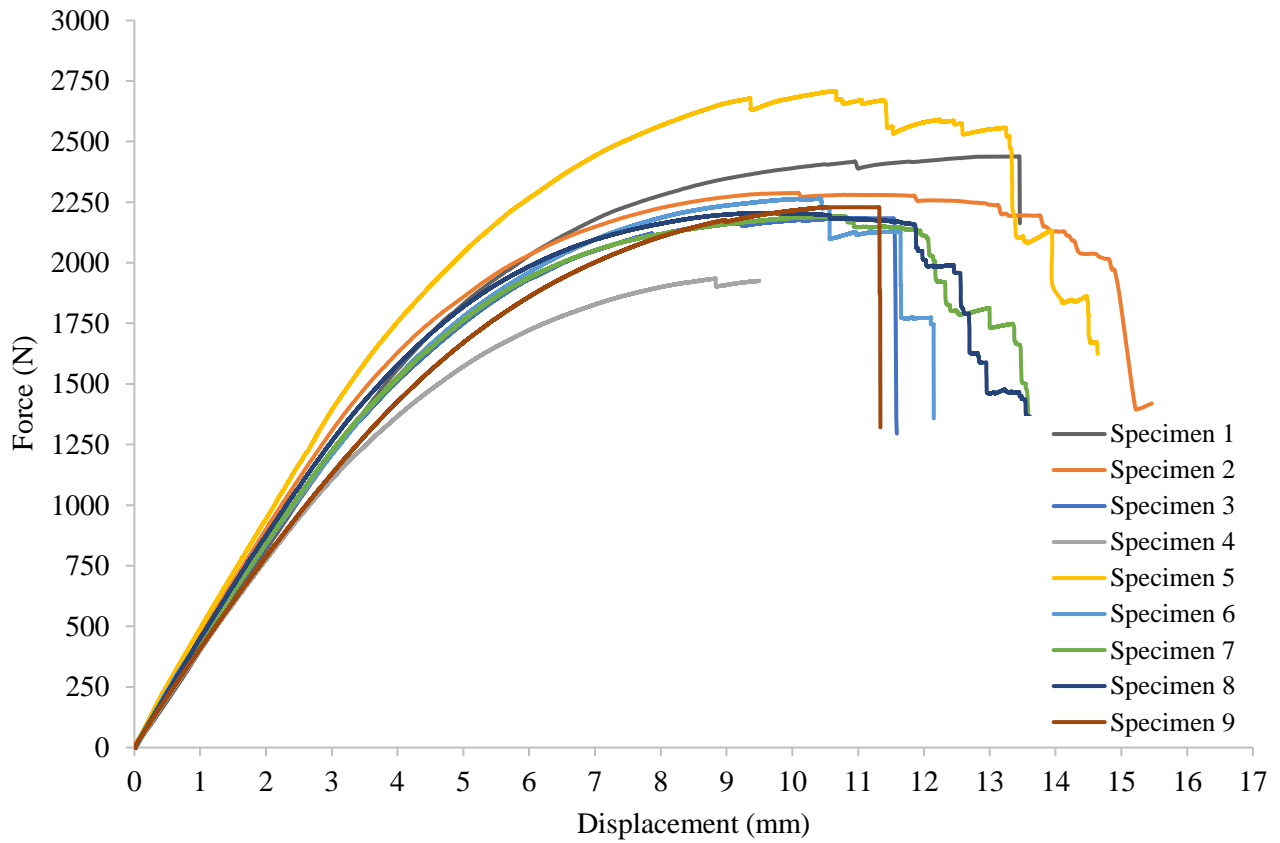


Figure 1. 9 Force-displacement curves for the static bending tests of clear wood samples

Table 1. 2 Summary of the results for static bending tests of clear wood samples

<b>Sample ID</b>	<b>MC %</b>	<b>MOE (GPa)</b>	<b>MOR (MPa)</b>
1	9.04	10.32	75.17
2	9.39	11.40	70.51
3	9.34	10.90	67.32
4	8.97	10.04	59.60
5	8.53	12.28	83.45
6	8.74	11.12	69.76
7	9.04	10.67	67.53
8	8.89	11.35	67.95
9	9.27	10.06	68.68
<b>Mean</b>	<b>9.02</b>	<b>10.91</b>	<b>70.00</b>
<b>SD</b>	<b>0.28</b>	<b>0.73</b>	<b>6.48</b>
<b>COV</b>	<b>3.14%</b>	<b>6.67%</b>	<b>9.25%</b>

### 1.6.1.2 CLT Flexural Tests Results

The  $MOE_{CLT}$  and  $MOR_{CLT}$  of the CLT were calculated for each specimen. The mean and SD of  $MOE_{CLT}$  and  $MOR_{CLT}$  were  $9.14 \pm 1.65$  GPa and  $39.16 \pm 6.59$  MPa with a COV of 18.01 % and 16.84 %, respectively. Also, the proportional limit (PL) was obtained for all tested specimens and the average value was 4.42 kN with a COV of 12.27%. This proportional limit was used in the next chapter, creep behavior testing.

The density and MC for each specimen were measured. A small section near the failure point was cut to determine the density and moisture content. The mean and SD of MC were  $12.01 \pm 0.18$  % with a COV of 1.47%. A summary of the results is presented in Table 1.3.

Table 1. 3 Summary of the flexural tests results of CLT beams

<b>CLT ID</b>	<b>MC %</b>	<b>MOE<sub>CLT</sub> (GPa)</b>	<b>MOR<sub>CLT</sub> (MPa)</b>	<b>PL (kN)</b>	<b>Density (kg/m<sup>3</sup>)</b>
1	12.0	9.30	39.84	4.60	485
2	11.8	10.52	43.01	4.20	488
3	11.8	6.35	28.18	3.70	532
4	12.3	11.05	45.02	5.10	449
5	12.1	8.75	34.59	4.00	445
6	12.0	8.90	44.30	4.90	498
<b>Mean</b>					
	<b>12.01</b>	<b>9.14</b>	<b>39.16</b>	<b>4.42</b>	<b>483</b>
<b>SD</b>					
	<b>0.18</b>	<b>1.65</b>	<b>6.59</b>	<b>0.54</b>	<b>32.21</b>
<b>COV</b>					
	<b>1.47%</b>	<b>18.01%</b>	<b>16.84 %</b>	<b>12.27%</b>	<b>7.00%</b>

The failure modes of three CLT beams are shown in Figure (1.10). Shear and rolling shear failure modes were observed after the third point bending tests in all tested specimens. However, a combination of tension and rolling shear failures were observed in two specimens as shown in specimen 3.

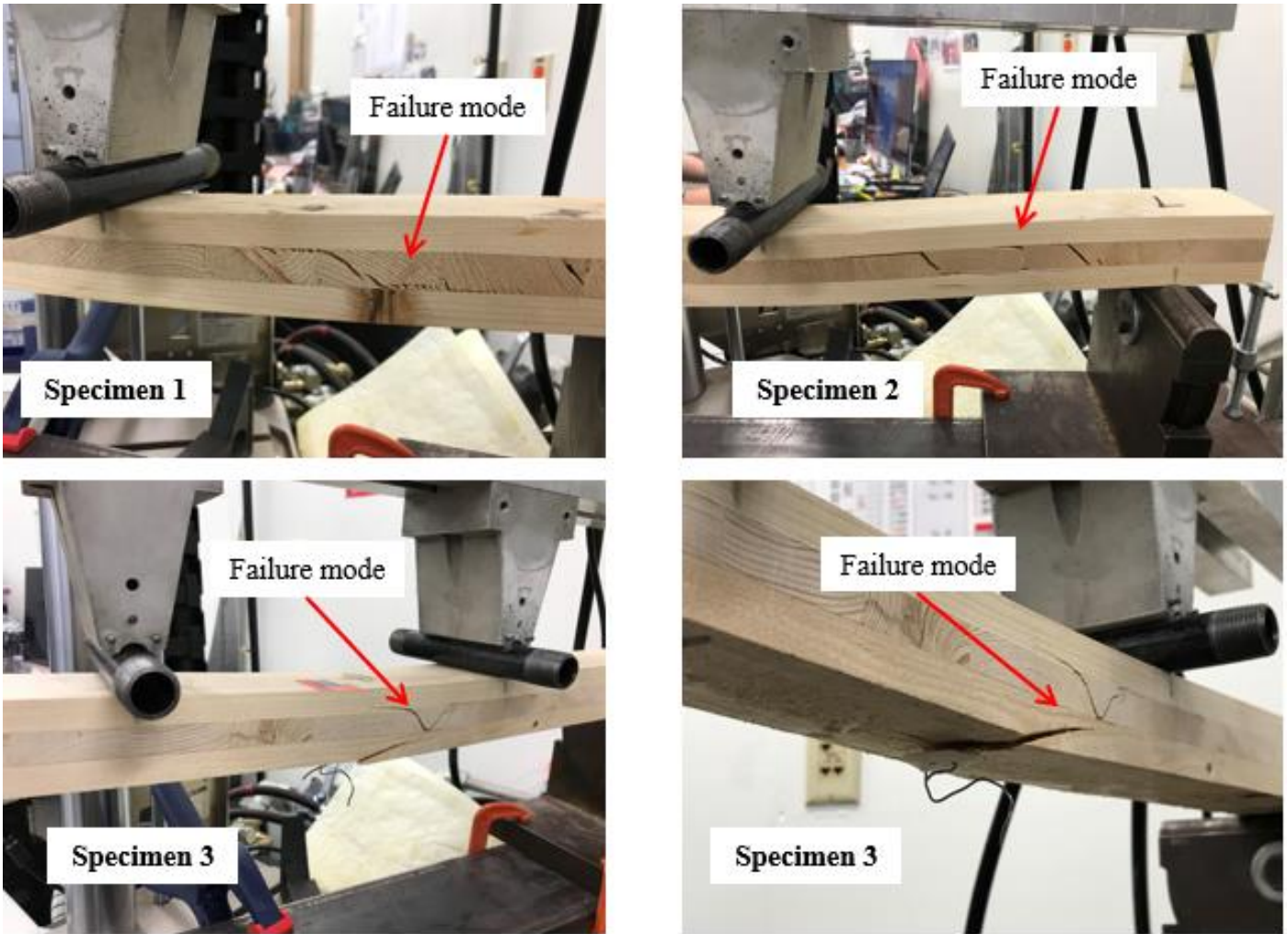


Figure 1. 10 Failure modes of some CLT specimens

## 1.6.2 Numerical Results

### 1.6.2.1 Elastic Properties Computations

The MOE in the longitudinal direction was determined experimentally as presented in Section 1.6.1.1. The experimental value of MOE was obtained by performing static bending tests using clear spruce wood specimens. The average value of MOE was used to calculate the other elastic properties by using Bodig and Jayne [17] relationship and Equation (1.7), which are presented in Section 1.4.1. The material properties of spruce wood, which are used for the numerical simulations, are estimated, and presented in Table 1.4.

Table 1. 4 The elastic properties of Spruce

Elastic properties	Value	Source
$E_L$ (GPa)	10.91	Experiment
$E_T$ (GPa)	0.5453	Bodig & Jayne relationship
$E_R$ (GPa)	0.8724	
$\nu_{RT}$	0.558	
$\nu_{RL}$	0.038	Santaoja et al. [26]; Mirianon et al. [27]
$\nu_{TL}$	0.015	
$\nu_{LT}$	0.300	
$\nu_{LR}$	0.475	Equation [1.7]
$\nu_{TR}$	0.349	
$G_{LT}$ (GPa)	0.7322	
$G_{LR}$ (GPa)	0.7789	Bodig & Jayne relationship
$G_{RT}$ (GPa)	0.0779	

### 1.6.2.2 Flexural Simulation Results

The numerical flexural force-deflection response for the 3-ply CLT beam is shown in Figure (1.11) and compared with experiment. The presented average experimental curve is for the two specimens presented in the figure since the full data was recorded only for these two specimens. As shown in the figure, the simulation response is slightly under predicted compared to the average response of the experiment. Also, based on the implemented damage model, the non-linear region was not captured as seen in the experimental curves.

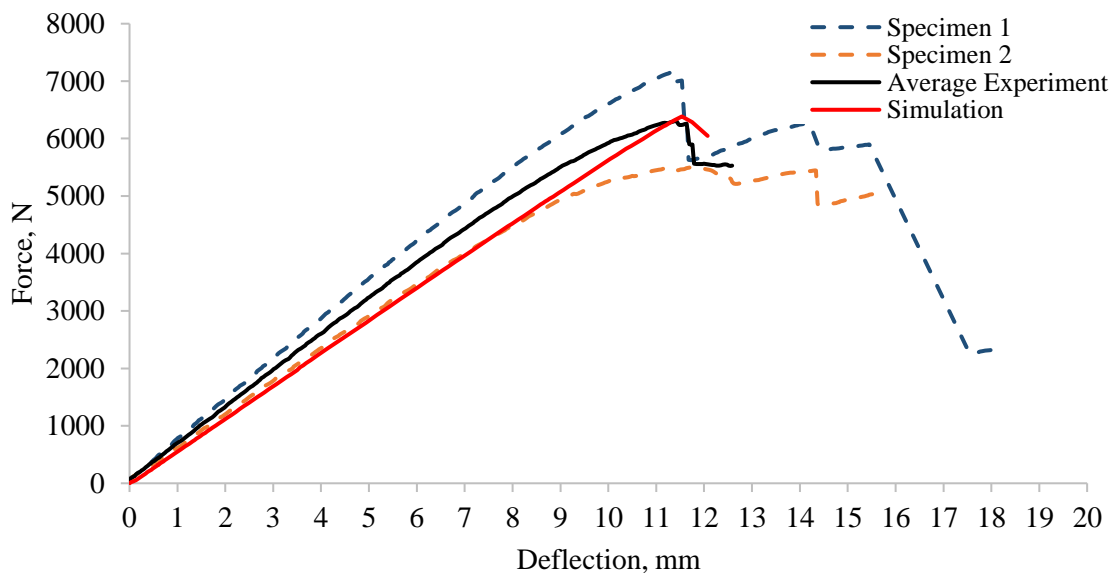


Figure 1. 11 Numerical flexural force-displacement response of CLT beam compared to experiment

The elastic properties are validated with experiment by predicting the CLT flexural modulus  $E_L^{fl}$  using the classical laminated theory. This validation is performed to ensure that the estimated elastic properties in Table 1.4 predict the CLT modulus close to the experimental value. The experimental CLT bending modulus was determined in Section 1.6.1.2 and presented in Table 1.3. The experimental value is the average of six specimens. To predict the CLT flexural modulus  $E_L^{fl}$ , the theoretical expressions are illustrated in Section 1.5, and Equation (1.14) was used. Table 1.5 summarizes the flexural modulus results of experiment, simulation, and theoretical results of the CLT bending modulus. As shown in the results, there is a 14.18 % difference between experiment and theory. As known, wood is a natural composite material, and many factors influence its properties. Thus, the experiment results are influenced by the moisture content of the wood, and some defects that could be present in the wood but not accounted for in the classical laminate theory prediction. However, the FE CLT model predicted  $E_L^{fl}$  and MOR, and the simulated results showed good correlation with experiment with a difference of 5.10% and 2.41%, respectively.

Table 1. 5 Summary of the modulus of elasticity and modulus of rupture of the CLT beam

	<b>Experimental</b>	<b>Simulation (%Difference)</b>	<b>Theory (%Difference)</b>
$E_L^{fl}$ (GPa)	9.14	8.69 (5.10%)	10.54 (14.18%)
<b>MOR (MPa)</b>	39.16	40.11 (2.41%)	-

## 1.7 Conclusion

The flexural response of thin CLT beams was investigated using experiment and computational simulations. Third point bending tests of CLT beams were carried out in accordance with ASTM D198. Material properties of Spruce wood were determined and the flexural response of CLT beams was presented. In addition to the experiment work, a finite element model of CLT beam was developed to analyze its behavior under flexural loading. A progressive damage model was adopted using the Hashin failure criterion to predict the failure and damage mechanism of timber.

The numerical results were validated by comparison with the experimental results. Excellent agreement was observed in terms of the MOE and MOR of the CLT beam between the numerical model and experiment. The numerical and experimental MOE were 8.69 GPa and 9.14 GPa, respectively with a difference of 5.10 %. In regards of MOR, the numerical and experimental values were 40.11 MPa and 39.16 MPa, respectively with a difference of 2.41%.

The current FE model could be improved by defining plasticity along with the Hashin failure criterion to illustrate a better prediction of the non-linear region of the flexural response of the CLT beam. Another important improvement that needs to be made to the numerical model is to adopt a criterion, i.e., using cohesive elements tool available in ABAQUS, to model as well as evaluating the adhesive layer or/and delamination between layers. This would help to accurately capture the flexural response and failure mechanisms.

## CHAPTER 2: Creep Performance of Scaled-Down Cross-Laminated Timber Beams Under Elevated Relative Humidities

### 2.1 Introduction

For timber buildings to be used for their entire intended lifespan, it is necessary to guarantee both the load capacity and the serviceability of buildings. During the building service life, the structural element must support the short-term as well as the long-term (or permanent) loadings. In particular, permanent loads cause the resistance of the timber elements to decrease and deformation to increase (creep behavior). The long-term performance of wood is mostly affected by creep behavior. The typical creep deformation with time subjects to three stages: first stage, secondary state, and tertiary stage till failure [1] (Figure 2.1).

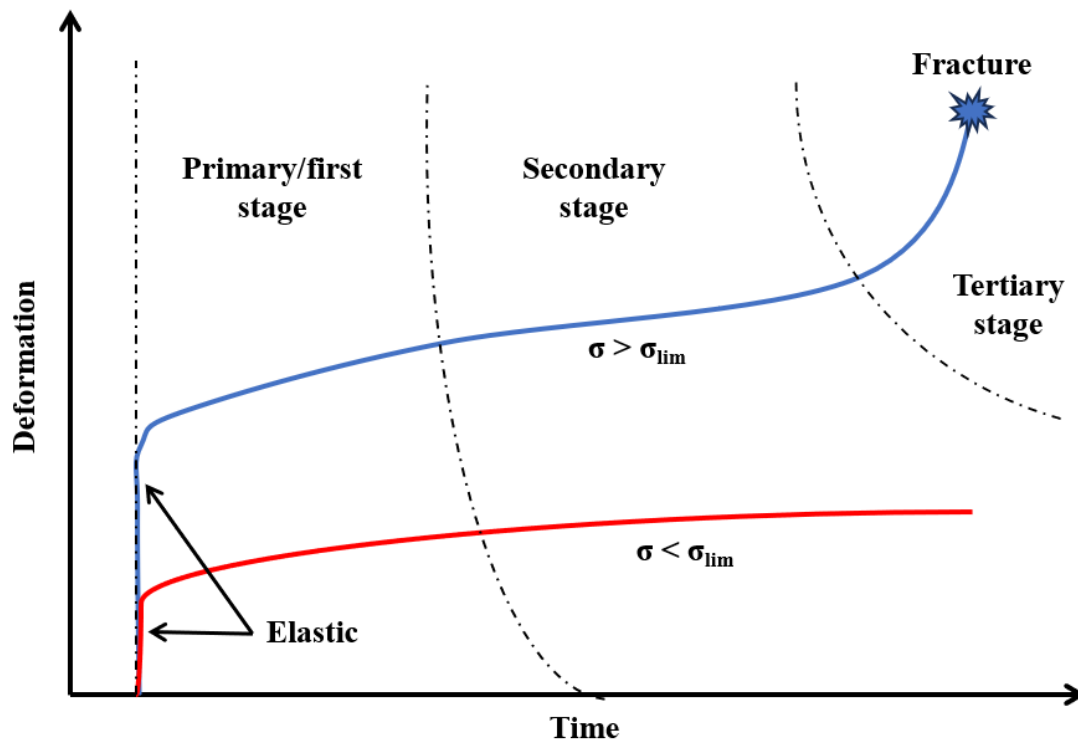


Figure 2. 1 Three phases of creep and the influence of stress loading on the evolution of deformation with time [27]

Creep in wood can be separated into two main categories, viscoelastic creep and mechano-sorptive creep. Viscoelastic creep is defined as the deformation with time at constant load under constant environmental conditions, i.e., constant temperature and relative humidity (RH). Also, it is named normal creep [2] which typically shows continuous increase in creep deformation with time as shown in Figure 2.1. The normal creep has been the subject of many investigations, which have examined the influence of stress ([3] and [4]), temperature [5], and moisture content [6]. The normal creep behavior of wood and wood plastic composites has long been studied using the widely accepted Burgers model ([7], [3], and [8]) in rheology theory (Figure 2.2) in a combination of experimental measurements. Rheology is the study of the flow of matter and rheological models can be used to describe time-dependent viscoelastic behavior of viscoelastic materials, including timber, polymers, and adhesives. As seen in Figure 2.2, the Burgers model combines a Maxwell model and a Kelvin model connected in series, which consist of spring and dashpot elements ([9] and [10]).

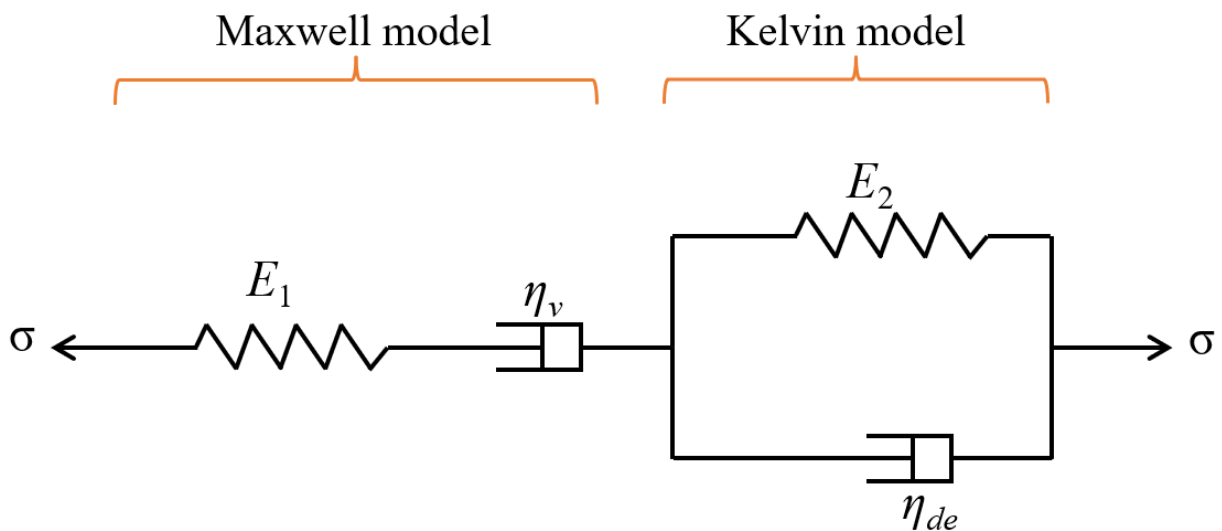


Figure 2. 2 Schematic diagram of four-element Burgers model [3, 7, 8]

Mathematically, the four-element Burgers model is often expressed as follows [2]:

$$\varepsilon(t) = \varepsilon_e + \varepsilon_{de} + \varepsilon_v = \sigma \left[ \frac{1}{E_e} + \frac{1}{E_{de}} \left[ 1 - \exp\left(-\frac{E_{de}}{\eta_{de}} t\right) + \frac{t}{\eta_v} \right] \right] \quad [2.1]$$

where  $\varepsilon$  is the total creep strain;  $\varepsilon_e$ ,  $\varepsilon_{de}$  and  $\varepsilon_v$  are elastic strain, viscoelastic strain and viscous strain, respectively.  $\sigma$  is stress,  $E_e$  is instantaneous modulus of elasticity,  $E_{de}$  is modulus of viscoelasticity,  $t$  is time after loading,  $\eta_{de}$  is viscosity of Kelvin-Voigt dashpot in Burgers model and  $\eta_v$  is viscosity of Maxwell dashpot in Burgers model. The effectiveness of the Burgers model and modified model on the normal creep has been examined by many researchers. As stated, this viscoelastic model is only valid with the assumptions of constant temperature and RH conditions.

However, the temperature and relative humidity (RH) in the environment are always changing over time, resulting in timber/wood structures absorbing or desorbing moisture throughout their service life. When the timber/wood is under a constant loading condition, creep deformation that occurs in varying RH and temperature environment is called mechano-sorptive creep [2]. The mechano-sorptive impact has the potential to greatly accelerate the creep deflection of a timber element and cause failure in a variety of environmental conditions ([11], [12], [13], and [14]). In Figure 2.3, we can observe that while the overall trend of creep deformation is increasing over time, there is a noticeable rapid increase in creep deformation during moisture desorption with the drop in RH (i.e., from 89% to 42%), aside from the initial RH increase, and a slight decrease in creep deformation during moisture adsorption with the increase in RH (i.e., from 42% to 89%) [14]. This poses a challenge in designing the deflection limits of timber structures over their lifespan due to the fact that wood is a hygroscopic material, which causes the Burgers model to underestimate the creep deformation. Therefore, the prediction of long-term creep effects is of

crucial importance to structural engineers when designing timber structures, considering ambient relative humidity and temperature fluctuations.

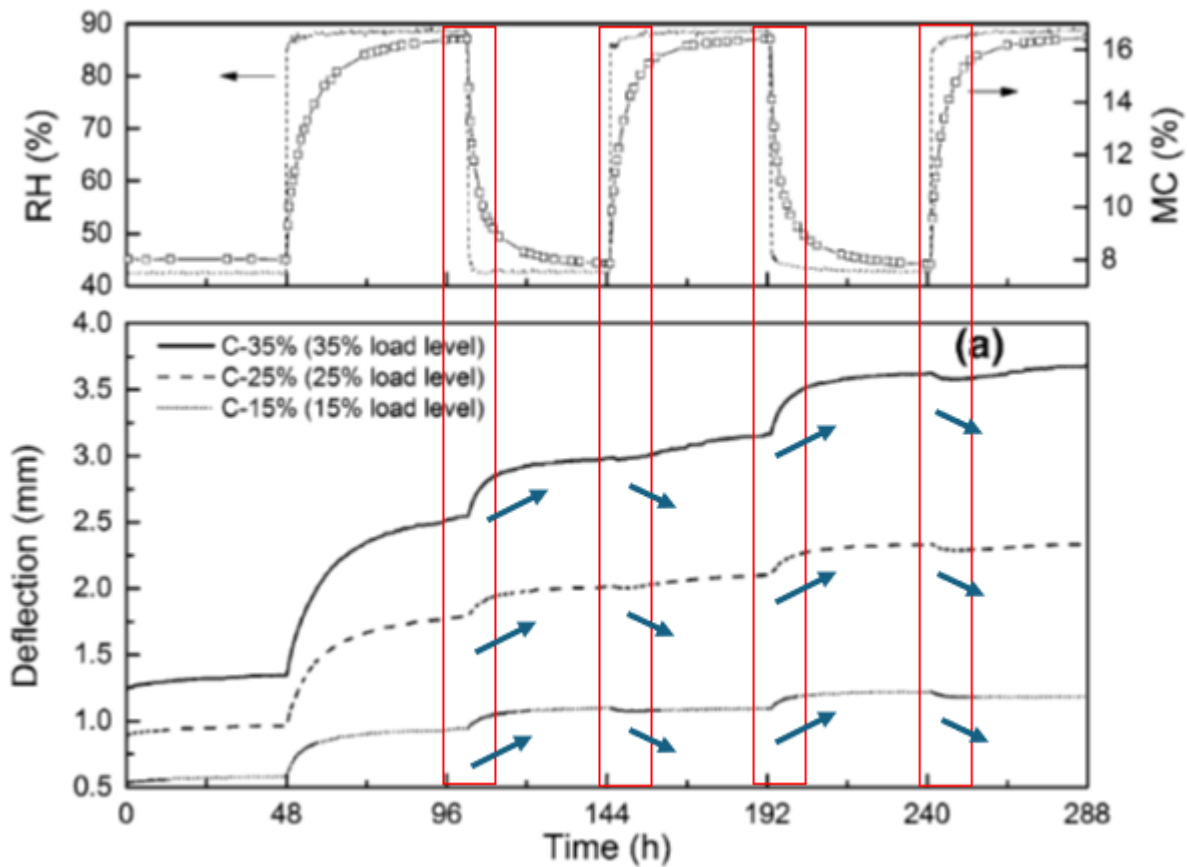


Figure 2. 3 Creep deflection of poplar (*Populus euramevicana*) under the RH cycles of 42%-89%-42% [14]

To solve this challenge, researchers at the Technical Research Centre of Finland (VTT) first developed a numerical analysis method to simulate creep deformation of wood using ABAQUS [15]. The VTT analysis method is suitable for problems where the mechano-sorptive creep has a major influence on the total deformation. The VTT method was developed to evaluate three strain components, linear elastic strain, free moisture expansion, and mechano-sorptive creep. The viscoelastic creep was excluded because of computational difficulties, and its influence on the results compared to the mechano-sorptive creep was not noticeable. There is an effort put into the computational simulations of the hygro-mechanical creep behavior of timber elements as shown

in [10]. The authors developed a fully coupled moisture-stress finite element model to evaluate the viscoelastic, mechano-sorptive (recoverable and irrecoverable components), moisture-induced strains of fiber reinforced polymer reinforced timber elements when subjected to long-term and changes in relative humidity loads. An additional component was presented, modified irrecoverable mechano-sorptive strain, this component is expected to occur when there is increase in the moisture content of the timber to another level/percentage. The presented creep model showed an accurate prediction of the creep deflection of the CLT beams in both constant and variable environments.

This study was intended to evaluate the creep behavior of cross-laminated timber (CLT). CLT is a building system which is an interest in North American construction. CLT panels consist of several layers of lumber boards stacked crosswise (typically at 90 degrees). It is an engineered wood-based solution that complements the existing light frame and heavy timber options and is a suitable candidate for some applications that currently use concrete, masonry, and steel systems. CLT is an innovative wood product that was introduced in the early 1990s in Austria and Germany and has been gaining popularity in residential and non-residential applications in Europe [16]. A typical use of CLT panels is as load carrying plate in structural buildings such as walls, floors, and roofs. In the case of floors and roofs CLT panels, some important characteristics that must be considered are short-term and long-term behaviors such as creep deformation, instantaneous deflection, and the strength of panel for permanent loading.

Considering the layout of lumber pieces in CLT panels, their deflection may behave differently from that of a single piece of solid timber or lumber and glulam beams when subjected to constant mechanical loading and varying RH and temperature conditions. There is a lack of sufficient published information on the mechano-sorptive creep deformation of CLT beams. Therefore, this study aims to fill this knowledge gap. In this chapter, the goal was to develop a 3D finite element

(FE) model with detailed information to simulate the long-term mechano-sorptive creep behavior of CLT beams under a static bending condition and elevated RH levels. To achieve this goal, the following objectives were achieved:

- 1) Conduct a lab-scale creep experiment using the scaled-down CLT beams under a static bending and elevated RH levels of 30%, 60%, and 90%.
- 2) Develop an FE model to simulate transient moisture transfer in the CLT beam to obtain the moisture distribution profile with time.
- 3) Develop an FE model to simulate the mechano-sorptive creep behavior of the CLT beam with the increase of RH from 30% to 60%, and then to 90%, and validate the numerical creep deflection with experiment.

## **2.2 Experimental Creep Test Setup**

This section presents the setup, materials, instrumentations used, and loading and environmental conditions for the creep experiment. Two scaled down CLT beams were investigated to evaluate their creep behavior under different relative humidity (RH) levels for three months. The dimension of CLT beams was scaled down to ensure the testing could be carried out in a temperature and RH controlled environmental chamber with limited space.

### **2.2.1 Materials**

Spruce lumber sourced from the local supplier was used to fabricate the CLT beams for the creep behavior experiment. Loctite® PR 3105 PURbond primer and Loctite® PURbond HB X602 adhesive, from Henkel Adhesives, were used as the adhesive system for the CLT fabrication. Chapter 1, Section 1.2, illustrates detailed information for the determination of scaled-down factor, lumber preparation, primer and adhesives used, and CLT billet fabrication. The CLT beams were

cut from the master billet with dimensions of 63.5 mm (2.5 in.) x 38.1 mm (1.5 in.) x 787.4 mm (31 in.) (width x thickness x length).

### 2.2.2 Creep Testing Setup

The creep test was conducted using a third point bending test setup by placing the CLT specimens on a custom-made test frame. The configuration and geometry of the test specimens are illustrated in Figure 2.4. The span-to-depth ratio of CLT was 18. The specimens were supported by rounded wood bars from the two ends. The wood bars were mounted on the frame to prevent the bars from moving or rotating. The testing frame was placed in an environmental chamber as shown in Figure 2.5.

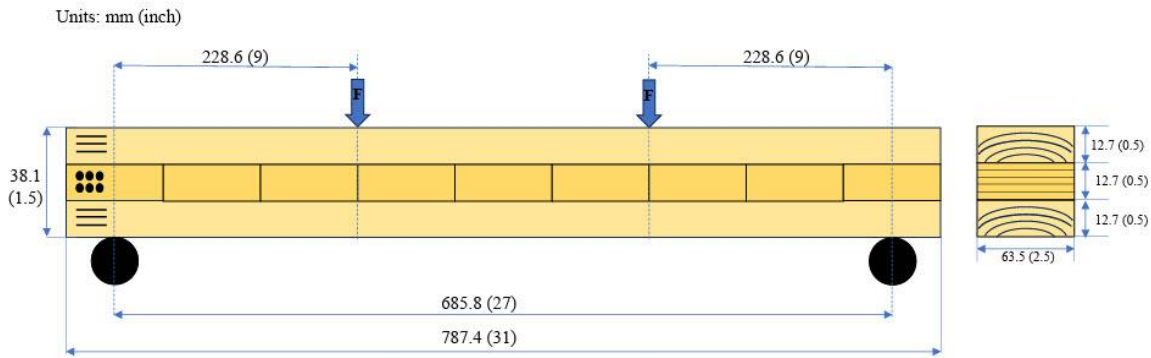


Figure 2. 4 Sketch of the test configuration and specimen's geometry



Figure 2. 5 Creep testing frame

### 2.2.3 Instrumentations

The instruments used for the creep behavior investigation included multiple channel portable data logger, linear variable inductive transducer (LVIT), Onset HOBO temperature/RH data logger, humidifiers, humidity controller, and power supply. LVIT position sensors from Omega<sup>TM</sup> with a range of 0 to 20 mm were used to measure the CLT beams deflection during the creep test. The LVIT devices were installed to measure the deflection from the center base of the specimens. The reading from the LVIT sensors was recorded using eight channels programmable data logger. Also, two humidifiers were placed inside the chamber and controlled using an INKBIRD humidity

controller. The temperature and RH inside the chamber were recorded for the entire duration of the test using Onset HOBO temperature/RH sensor.

#### **2.2.4 Environmental Conditions and Loading**

The creep test was performed in a conditioning chamber under 3 different RH levels, 30 %, 60 %, and 90 %. The total testing period was 3 months, the initial relative humidity (RH) was set at 30% for one month, then increased to 60% for another month, and finally to 90% for a third month.

The temperature of the chamber remained constant at  $22 \pm 2$  °C. Before starting the creep test, the chamber was checked for a couple days to ensure it reached the target initial RH and temperature.

Before the creep test, the CLT beams were conditioned in another environmental chamber at a constant temperature of  $23 \pm 2$  °C and RH of  $53 \pm 5$  % for about 8 weeks. The CLT beams were loaded with steel weights. The load level applied was 30% of the proportional limit (PL) of the CLT beams. The PL was obtained experimentally by performing flexural tests on similar CLT specimens, and the results of the flexural tests were presented in Chapter 1, Section 1.6.1.2. The average PL value was 4.417 kN from 6 tested CLT specimens. Therefore, a load of 1.325 kN (135 kg or 297 lbs.) was applied for each tested CLT beam. Steel chains were used to load or hang the weights on the CLT beams as shown in Figure 2.6.



Figure 2. 6 Experimental creep test setup

### **2.3 Numerical Model of Mechano-Sorptive Creep of CLT Beams**

In this section, the details of a 3-dimensional FE model are presented which is developed to simulate the long-term creep behavior of thin CLT beam. The numerical model intends to evaluate the total strain when subjected to external loadings and relative humidity changes with time. The FE model is developed using the finite element package ABAQUS [17].

### 2.3.1 Moisture Diffusion Model

The moisture diffusion process in the interior of wood material was assumed to follow Fick's law [18] as shown in Equation [2.2].

$$\left. \frac{\partial u}{\partial t} \right|_{\Omega} = \nabla(D \nabla u) \quad [2.2]$$

where  $u$  is the moisture content (MC) of wood,  $t$  is the time,  $D$  is the moisture diffusion coefficient, and the interior of the wood denoted by  $\Omega$ . The density of wood in this form of Fick's law was considered to be constant. For a more realistic description of moisture diffusion in 3D wood structures, the value of  $D$  in the three directions should be defined. The diffusion coefficients in the longitudinal direction  $D_L$  and transverse direction  $D_T$  were adopted in this study from Zhou et al. [19] and Fortino et al. [20], respectively. The expressions of  $D_L$  and  $D_T$  are presented in Equations [2.3] and [2.4], respectively. For the radial direction,  $D_R = D_T$  was assumed.

$$D_L(u) = 2.88 \times 10^{-7} e^{4u} \left( \frac{m^2}{h} \right) \quad [2.3]$$

$$D_R(u) = D_T(u) = 8.64 \times 10^{-7} e^{4u} \left( \frac{m^2}{h} \right) \quad [2.4]$$

Fick's law is analogous to Fourier's law of heat transfer. The expression of Fourier's law is presented in Equation [2.5].

$$\rho c_T \left. \frac{\partial T}{\partial t} \right|_{\Omega} = \nabla(\lambda \nabla T) \quad [2.5]$$

where  $\rho$ ,  $\lambda$ ,  $T$ , and  $c_T$  are the density, thermal conductivity, temperature, and specific heat of wood, respectively. Because of the relation between Fourier's law and Fick's law, the moisture diffusion

process can be simulated and analyzed in the finite element package ABAQUS. Therefore, the moisture diffusion and mechanical behavior assessment of wood material can be achieved by using the coupled temperature-displacement analysis step available in ABAQUS. Using the relation between Equations [2.2] and [2.5] and putting  $c_T = I$  and  $\lambda = \rho D$  to implement the moisture transfer process in ABAQUS and be able to perform moisture-stress investigation.

In the case of the rate of moisture flow between the surface of the wood and the surrounding environment is governed by the following expression:

$$q_n = \rho S_u (u_{EMC} - u_{surf}) \quad [2.6]$$

where  $q_n$  is the moisture flow across the boundaries,  $S_u$  is the coefficient of surface emission,  $u_{EMC}$  is the equilibrium moisture content of wood corresponding to the surrounding environment, and  $u_{surf}$  is the moisture content of the wood surface. The coefficient of surface emission,  $S_u$ , is a function of the moisture content,  $u$ , where it defines the rate of moisture content exchanged across the boundaries of wood. In the present work, the surface emission presented in Hanhijarvi [21],  $S_u = 1.152 \times 10^{-4} e^{4u}$  was used.

In the case of the equilibrium moisture content (EMC) of wood,  $u_{EMC}$ , there have been a lot of work to develop a mathematical equation of the  $u_{EMC}$  in the past few years. Toratti [4], Hanhijarvi [21], Becker [22], and Martensson [23] presented different expressions to evaluate the  $u_{EMC}$ .

- The EMC of wood expression according to Toratti is a function of RH as shown in the following equation:

$$u_{EMC} = \frac{0.01 \times RH}{-0.00084823 \times RH^2 + 0.11665 \times RH + 0.38522} \quad [2.7]$$

- The EMC of wood expression according to Hanhijarvi is a function of temperature, T, and RH as shown in the following equation:

$$u_{EMC} = 0.01 \left( \frac{-T \times \ln(1 - h)}{0.13[1 - T/647.1]^{-6.46}} \right)^{T^{0.75}/110} \quad [2.8]$$

where T is in Kelvin, and h = %RH/100.

- The EMC of wood expression according to Becker is an exponential function of RH as shown in the following equation:

$$u_{EMC} = 0.113 \times RH^{0.54} + 0.192 \times e^{-0.5(2.7(RH-1)-1)^2} + 0.09 \times e^{-0.5(20.5(RH-1)-1)^2} \quad [2.9]$$

- The EMC of wood expression according to Martensson is a function of RH as shown in the following equation:

$$u_{EMC} = 0.2439353898 \left( \frac{RH}{100} \right)^6 + 0.1276829904 \left( \frac{RH}{100} \right)^5 + 0.09340840267 \left( \frac{RH}{100} \right)^4 - 0.464828494 \left( \frac{RH}{100} \right)^3 + 0.1208946628 \left( \frac{RH}{100} \right)^2 + 0.1948280174 \left( \frac{RH}{100} \right) \quad [2.10]$$

The four expressions of the EMC of wood presented above in Equations [2.7] – [2.10] are plotted against experimental Dynamic Vapor Sorption (DVS) adsorption data of spruce tested at 25°C, see Figure 2.7.

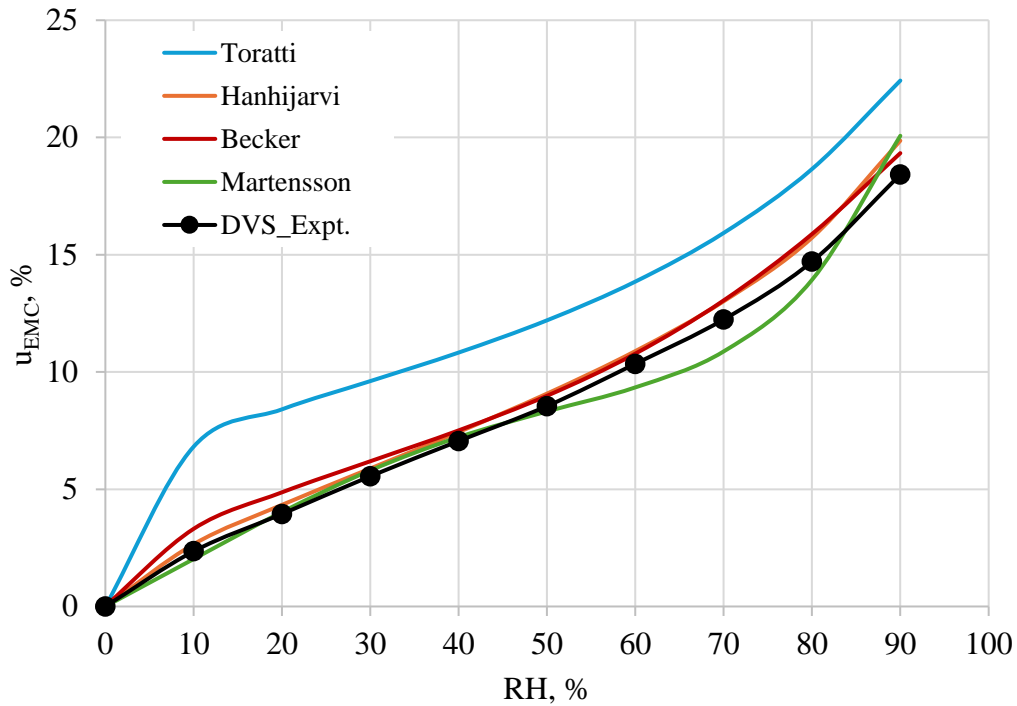


Figure 2. 7 Plot of the equilibrium moisture content of wood using different expressions

In this study, for the numerical model implementation, the equilibrium moisture content equation presented in Hanhijarvi [21] was adopted since its results correlate well with the DVS results. The load at the surface of the wood was implemented in ABAQUS through a DFLUX user subroutine to apply a defined time dependent relative humidity boundary condition.

### 2.3.2 Strain Components

The FE model was developed in ABAQUS to evaluate the total strain experienced in wood when subjected to mechanical loading, moisture content induced expansion or shrinkage loading, and temperature induced expansion or contraction loading. The total strain includes five separate strain components where the five strain components are solved using an incremental analysis with time.

The total strain,  $\epsilon_{total}$  expression is given in Equation [2.11].

$$\epsilon_{total} = \epsilon_e + \epsilon_T + \epsilon_u + \epsilon_{ms} + \epsilon_{cr} \quad [2.11]$$

where

$\varepsilon_e$  is the elastic strain component

$\varepsilon_T$  is the thermal strain component

$\varepsilon_u$  is the moisture induced strain component

$\varepsilon_{ms}$  is the mechano-sorptive strain component

$\varepsilon_{cr}$  is the creep strain component

### 2.3.2.1 Elastic Strain Component

The elastic strain,  $\varepsilon_e$  follows Hooke's law as illustrated in Equation[2.12].

$$\varepsilon_e = S_e \sigma \quad [2.12]$$

$$S_e = \begin{bmatrix} \frac{1}{E_R} & -\frac{\nu_{tr}}{E_T} & -\frac{\nu_{LR}}{E_L} & 0 & 0 & 0 \\ -\frac{\nu_{RT}}{E_R} & \frac{1}{E_T} & -\frac{\nu_{LT}}{E_L} & 0 & 0 & 0 \\ -\frac{\nu_{RL}}{E_R} & -\frac{\nu_{TL}}{E_T} & \frac{1}{E_L} & 0 & 0 & 0 \\ 0 & 0 & 0 & \frac{1}{G_{RT}} & 0 & 0 \\ 0 & 0 & 0 & 0 & \frac{1}{G_{RL}} & 0 \\ 0 & 0 & 0 & 0 & 0 & \frac{1}{G_{TL}} \end{bmatrix} \quad [2.13]$$

where  $\sigma$  is the stress vector,  $S_e$  is the orthotropic compliance matrix as presented in Equation [2.13].

The subscript in Equation [2.13]  $L$ ,  $T$ , and  $R$  refer to the longitudinal, tangential, and radial directions, respectively.  $E_i$ ,  $G_{ij}$ , and  $\nu_{ij}$  ( $i, j = L, T, \text{ and } R$ , and  $i \neq j$ ) are the modulus of elasticity, modulus of shear, and Poisson's ratio, respectively. Santaoja et al. [15] suggested adjusting the elastic and shear modulus properties in the numerical model when the environmental conditions are different from the referenced conditions. Therefore, the modulus of elasticity and shear in the

three directions,  $L$ ,  $T$ , and  $R$ , are assumed to be proportional to the density, temperature, and moisture content of wood as stated in Equation [2.14].

$$\begin{aligned} E_i &= E_{i,ref} [1 + \alpha_1(\rho - \rho_{ref}) + \alpha_2(T - T_{ref}) + \alpha_3(u - u_{ref})] \\ G_{ij} &= G_{ij,ref} [1 + \alpha_1(\rho - \rho_{ref}) + \alpha_2(T - T_{ref}) + \alpha_3(u - u_{ref})] \end{aligned} \quad [2.14]$$

where  $E_{i,ref}$  and  $G_{ij,ref}$  are the reference elastic and shear moduli, respectively, which correspond to the reference density  $\rho_{ref}$ , moisture content  $u_{ref}$ , and temperature,  $T_{ref}$ .  $\rho$ ,  $u$  and  $T$  denote to the current density, moisture content and temperature, respectively, at any given time step in the FE model.  $\alpha_1$ ,  $\alpha_2$ , and  $\alpha_3$  are modulus of elasticity increment coefficients in relation to density, temperature, and MC, respectively, where  $\alpha_1 = 0.003$ ,  $\alpha_2 = -0.007$  and  $\alpha_3 = -2.6$  were obtained from Santaoja et al. [15] and Mirianon et al. [24].

### 2.3.2.2 Moisture-Induced Strain Component

The moisture strain occurs when there is moisture change within the wood material. The moisture strain component is evaluated using the following expression:

$$\varepsilon_u = \alpha_u \nabla u \quad [2.15]$$

where  $\nabla u$  is the increment of moisture content, and  $\alpha_u$  is the moisture expansion coefficient in the three directions (radial [R], tangential [T], and longitudinal [L]) and it is illustrated in Equation [2.16]. The values of the moisture expansion coefficient are obtained from literature [10] and presented in Table 2.1.

$$\alpha_u = [\alpha_{u,R} \quad \alpha_{u,T} \quad \alpha_{u,L} \quad 0 \quad 0 \quad 0]^T \quad [2.16]$$

### 2.3.2.3 Thermal Strain Component

The thermal-induced strain is evaluated using Equation [2.17].

$$\varepsilon_T = \alpha_T \nabla T \quad [2.17]$$

where  $\nabla T$  is the increment of temperature, and  $\alpha_T$  is the thermal expansion coefficient in the three directions (radial [R], tangential [T], and longitudinal [L]) and it is illustrated in Equation [2.18].

The values of the moisture expansion coefficient are obtained from literature [19] and presented in Table 2.1.

$$\alpha_T = [\alpha_{T,R} \quad \alpha_{T,T} \quad \alpha_{T,L} \quad 0 \quad 0 \quad 0]^T \quad [2.18]$$

It is stated that the temperature in the creep experiment was set at a constant temperature of 22°C with slight fluctuations within  $\pm 2^\circ\text{C}$ . The influence of temperature induced wood expansion or contraction is the least. However, it has remained in the equation of total strain calculation to demonstrate the FE model developed to be a general model.

### 2.3.2.4 Mechano-Sorptive Strain Component

Mechano-sorptive strain occurs only when moisture condition is changing. Therefore, in this case, the mechanical behavior is moisture rate dependent, and the performance will be a function of its past history at any moisture content under load. The mechano-sorptive strain component is evaluated using the expression found in Santaoja et al. [15] and illustrated in Equation [2.19].

$$\varepsilon_{ms} = \int_0^t S_{ms} \sigma \dot{u} dt \quad [2.19]$$

where  $S_{ms}$  is the mechano-sorptive compliance matrix and  $\dot{u}$  is the moisture content rate.  $S_{ms}$  comes in two forms depending on the sign of  $\dot{u}$ . The two forms of  $S_{ms}$  are shown in Equation [2.20].

$$S_{ms} = \begin{cases} S_{ms}^+ & \dot{u} > 0 \\ S_{ms}^- & \dot{u} \leq 0 \end{cases} \quad [2.20]$$

where  $S_{ms}^+$  and  $S_{ms}^-$  are obtained from Santaoja et al. [15] and shown in Equation [2.21].

$$S_{ms}^+ = \begin{bmatrix} 0 & 0 & 0 & 0 & 0 & 0 \\ 0 & 0 & 0 & 0 & 0 & 0 \\ 0 & 0 & -4 & 0 & 0 & 0 \\ 0 & 0 & 0 & 0 & 0 & 0 \\ 0 & 0 & 0 & 0 & -8 & 0 \\ 0 & 0 & 0 & 0 & 0 & -8 \end{bmatrix} \times 10^{-9} Pa^{-1} \quad [2.21]$$

$$S_{ms}^- = \begin{bmatrix} -10 & 10 & 0 & 0 & 0 & 0 \\ 10 & -20 & 0 & 0 & 0 & 0 \\ 0 & 0 & -0.05 & 0 & 0 & 0 \\ 0 & 0 & 0 & -100 & 0 & 0 \\ 0 & 0 & 0 & 0 & -1 & 0 \\ 0 & 0 & 0 & 0 & 0 & -1 \end{bmatrix} \times 10^{-8} Pa^{-1}$$

### 2.3.2.5 Creep Strain Component

The creep strain can be evaluated using the expression presented in Zhou et al. [19], and it is defined as follows:

$$\varepsilon_{cr} = \int_0^t S_{cr}(t) \frac{d\sigma(t')}{dt'} dt' \quad [2.22]$$

where  $S_{cr}(t)$  is the creep compliance matrix.  $S_{cr}(t)$  can be evaluated using Ormarson's approach [25] which describes the creep behavior of Kelvin-Chain body, and the expression is as follows:

$$S_{cr}(t) = \sum_{n=1}^N \varphi_n \left(1 - e^{-\left(\frac{t}{\tau_n}\right)}\right) S_e = R_c S_e \quad [2.23]$$

where  $R_c$  is the relative creep,  $N$  is the number of Kelvin elements,  $\varphi_n$  is the series factor, and  $\tau_n$  is the retardation time. In the current study, the creep strain was excluded from evaluating the total strain due to the lack of parameters needed to evaluate the creep strain, which are often obtained from empirical model by doing a creep test under constant temperature and RH. The current experimental design had a limitation, it lacked this type of creep testing. Also, the creep strain can be negligible because its influence is not noticeable as the mechano-sorptive strain [26].

### 2.3.3 ABAQUS User-Subroutine UMAT

The user-defined subroutine UMAT was originally encoded by Santaoja et al. [15] and it was adopted in this study with some modifications to define the material behavior such as the elastic, moisture, thermal, and mechano-sorptive strains. All the formulations in Section 2.3.2 are evaluated in UMAT subroutine. For more details on the implementation of UMAT can be found in Santaoja et al. [15] and Zhou et al. [19].

### 2.3.4 Numerical Model Development

#### 2.3.4.1 Model Geometry

A 3-dimensional FE coupled moisture-displacement model was developed in ABAQUS to assess the creep behavior of scaled down CLT beams under elevated RHs. The FE CLT model consisted of 3 layers ( $0^\circ$ ,  $90^\circ$ ,  $0^\circ$ ), and it was developed with 3D deformable solid elements. The dimensions of the CLT beam were 63.5 mm x 38.1 mm x 787.4 mm (width x thickness x length). The material orientation of the plies was defined using the available tool in ABAQUS. A local coordinate system was defined for each ply. Then, each ply was assigned a material orientation based on the local coordinate system of the ply.

The FE CLT beam was meshed using the coupled temperature-displacement elements. The element type used was the 8-node thermally coupled brick, trilinear displacement, and temperature C3D8T. Fully integrated elements were used with number of elements of 83,790.

The numerical creep simulation setup was similar to the experimental creep test setup which is illustrated in Figures 2.4 and 2.6. However, in the numerical model, the solid cylindrical supports were omitted to simplify the numerical model and try to reduce the computational time.

#### **2.3.4.2 Material Properties**

The elastic properties used were determined and presented in Chapter 1, Section 1.6.2.1. The material data of timber implemented in the numerical model are summarized in Table 2.1.

Table 2. 1 Material properties of timber implemented in the numerical model

<b>Notation</b>	<b>Description</b>	<b>Value</b>	<b>Source</b>
<b>E<sub>L</sub> (GPa)</b>	Longitudinal MOE	10.905	Experiment
<b>E<sub>T</sub> (GPa)</b>	Tangential MOE	0.5453	Bodig & Jayne relationship [1]
<b>E<sub>R</sub> (GPa)</b>	Radial MOE	0.8724	
<b><math>\nu_{RT}</math></b>	Poisson's ratio radial-tangential	0.558	Santaoja et al. [15] and Mirianon et al. [24]
<b><math>\nu_{RL}</math></b>	Poisson's ratio radial-longitudinal	0.038	
<b><math>\nu_{TL}</math></b>	Poisson's ratio tangential-longitudinal	0.015	
<b><math>\nu_{LT}</math></b>	Poisson's ratio longitudinal-tangential	0.300	Equation [1.7]
<b><math>\nu_{LR}</math></b>	Poisson's ratio longitudinal-radial	0.475	
<b><math>\nu_{TR}</math></b>	Poisson's ratio tangential-radial	0.349	
<b>G<sub>LT</sub> (GPa)</b>	longitudinal-tangential shear modulus	0.7322	Bodig & Jayne relationship [1]
<b>G<sub>LR</sub> (GPa)</b>	longitudinal-radial shear modulus	0.7789	
<b>G<sub>RT</sub> (GPa)</b>	radial-tangential shear modulus	0.0779	
<b><math>\rho_{ref}</math> (kg/m<sup>3</sup>)</b>	Reference density	400	O'Ceallaigh et al. [10]
<b>T<sub>ref</sub> (°C)</b>	Reference temperature	20	
<b>u<sub>ref</sub> (%)</b>	Reference moisture content	12	
<b>u<sub>FSP</sub> (%)</b>	Fiber saturation point	28	
<b><math>\alpha_1</math> (m<sup>3</sup>/kg)</b>	Density coefficient	0.0003	Santaoja et al. [15] and Mirianon et al. [24]
<b><math>\alpha_2</math> (1/°C)</b>	Temperature coefficient	-0.007	
<b><math>\alpha_3</math></b>	Moisture content coefficient	-2.6	
<b><math>\alpha_{u,L}</math></b>	Longitudinal moisture expansion coefficient	0.0122	O'Ceallaigh et al. [10]
<b><math>\alpha_{u,T}</math></b>	Tangential moisture expansion coefficient	0.2525	
<b><math>\alpha_{u,R}</math></b>	Radial moisture expansion coefficient	0.1371	
<b><math>\alpha_{T,L}</math> (1/°C)</b>	Longitudinal thermal expansion coefficient	3.75x10 <sup>-6</sup>	Zhou et al. [19]
<b><math>\alpha_{T,T}</math> (1/°C)</b>	Tangential thermal expansion coefficient	33.75x10 <sup>-6</sup>	
<b><math>\alpha_{T,R}</math> (1/°C)</b>	Radial thermal expansion coefficient	24.35x10 <sup>-6</sup>	
<b>D<sub>L</sub>(u) (m<sup>2</sup>/h)</b>	Diffusion coefficient in longitudinal	2.88 x 10 <sup>-7</sup> e <sup>4u</sup>	Fortino et al. [20]
<b>D<sub>R</sub>(u) = D<sub>T</sub>(u) (m<sup>2</sup>/h)</b>	Diffusion coefficient in Radial & Tangential	8.64 x 10 <sup>-7</sup> e <sup>4u</sup>	

### 2.3.4.3 Boundary Conditions

The FE model was developed to represent a third-point bending test setup. The boundary conditions applied to the FE model are shown in Figure 2.8. The FE CLT beam was simply supported with two constraints included to prevent the CLT beam translating and rotating in the other directions (Y and Z directions) but allow the beam to deflect. Additionally, a constant load of 1.325 kN was applied, which is 30 % of the proportional force/stress limit found and presented in Chapter 1.

An initial moisture content of 12 % was assigned to all the nodes of the FE model because the CLT beam specimens were conditioned in the environmental chamber at  $23 \pm 2$  °C and  $53 \pm 5$  % RH with a corresponding EMC of 12% before testing. As a hygroscopic material, the ambient temperature and RH change can result in MC of wood to reach a new EMC, creating moisture flux in or out of the wood. The interaction between CLT beam surface and ambient temperature and RH was achieved by defining a time-dependent RH load which was applied through the exposed surfaces of the beam. The exposed surfaces include all six surfaces of the FE beam. The RH loading profile was the same as the experimental setup. It was achieved by implementing the moisture diffusion model presented in Section 2.3.1 in ABAQUS by using a user defined subroutine DFLUX.

Also, although the temperature was set at 22°C, slight temperature fluctuations still occurred in the environmental chamber, its influence was also considered in the FE model with some simplifications. First, the initial temperature of 23 °C was assigned to the all the nodes of the FE CLT beam. Then, a time-dependent temperature load of  $22 \pm 2$  °C in terms of a Sine wave curve (initial amplitude of 22 °C and frequency of 0.5236 rad/hour) was assigned to all nodes of the elements of the CLT beam and it should be noted that all surfaces of the beam were exposed to the ambient environment. This was achieved by creating a Predefined Field in ABAQUS.

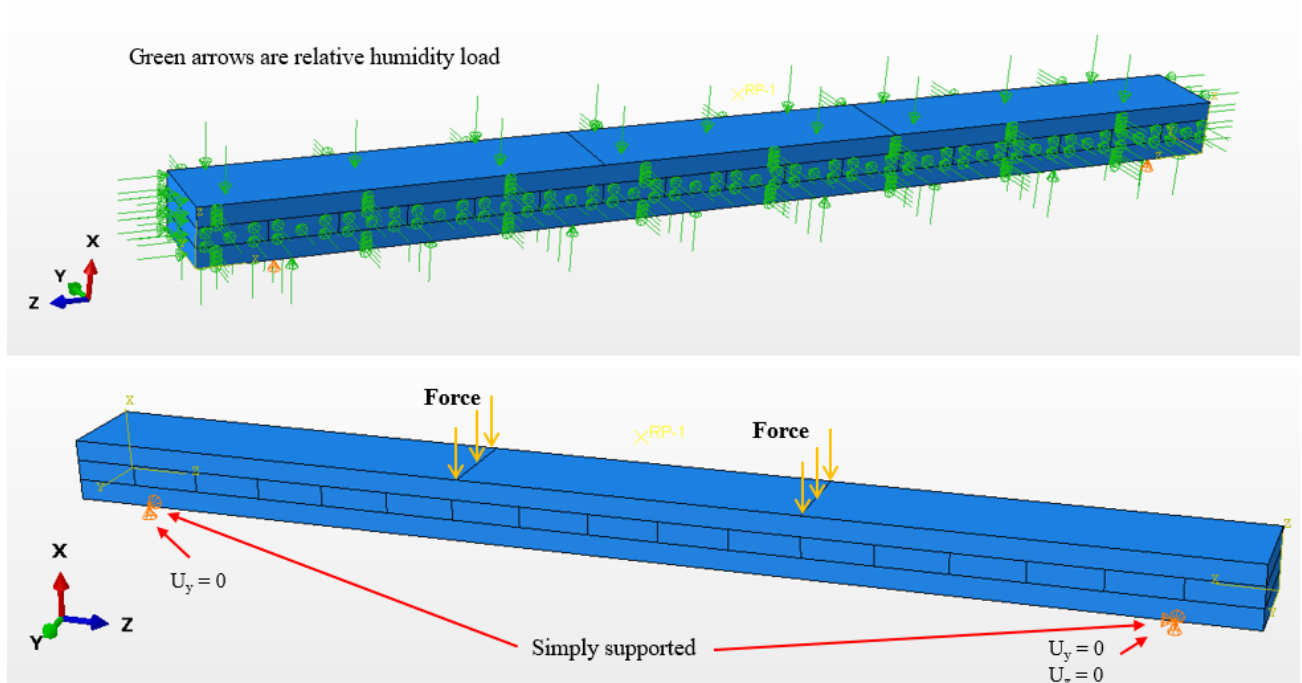


Figure 2. 8 The boundary conditions used in the numerical model

## 2.4 Results and Discussion

### 2.4.1 Experimental Results

The experimental results of the monitored temperature and RH of the environmental chamber and the creep deflection of scaled-down CLT beams are shown in Figures 2.9 and 2.10, respectively. As seen in Figure 2.9, the temperature remained around 22 °C with a slight decrease of 1 to 2 °C over the three-month period. The large upward spikes seen in the temperature curve might be caused by either unplanned power outages or times when the environmental chamber had to be opened to assess the assembly. In contrast, the RH of the environmental chamber was well controlled within a small variation of  $\pm 5\%$  by the two humidifiers at three target levels of 30%, 60%, and 90%. Some significant downward spikes were observed, possibly due to a malfunction in one of the two humidifiers or due to a power outage.

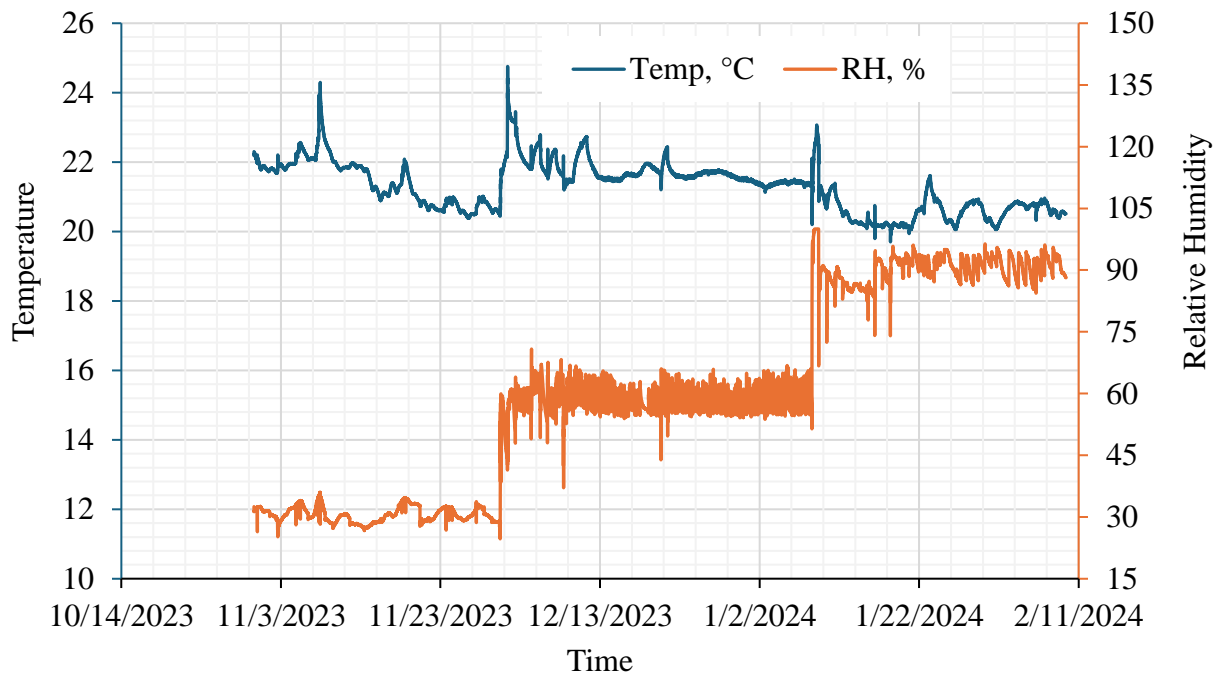


Figure 2. 9 Temperature and relative humidity of the testing chamber

Figure 2.10 presents the deflection results of two CLT beams along with the average data of the two beams. The overall trend of the creep deflection of two beams increased over time after the instant elastic deformation. Although the two CLT beams were cut from two different locations of the same CLT panel, beam 2 (blue, solid line) shows a larger deflection compared to beam 1 (red, solid line). This is due to the difference in the modulus of elasticity (MOE), beam 1 is stiffer with an MOE of 8.0 GPa and beam 2's MOE is 6.4 GPa. The MOE was obtained using the load at the 30% of PL and the corresponding instant elastic deflection measured by LVIT. It is pointed out that the CLT beams were conditioned at  $23 \pm 2$  °C and  $53 \pm 5\%$  RH, which corresponding EMC is about 12%. When the beams were placed in the chamber at a RH of 30% for one month, the CLT beams were subjected to a moisture desorption process, i.e., a decrease in moisture content. If the CLT beams could reach an equilibrium status, the moisture content of the CLT beams should be around 5 to 6 % MC (Figure 2.7). Then in the following two stages of 60% RH and 90% RH, only

moisture adsorption occurred in the CLT beams, the corresponding EMC of the CLT beams at 60% RH and 90% RH should be around 12% and 18%, respectively (Figure 2.7).

It should be noted that when the first moisture adsorption occurred as the RH was increased from 30% RH to 60% RH, the two CLT beams showed a slight decrease in deflection to different degrees in a very short period, as seen in the local area of A. Then creep deflection was recovered to increase, and the big increase noticed in deflection in the local area of B for the CLT beam 2. This is due to the readjustment of the LVIT extension rod, which was stuck for a certain amount of time. When the second moisture adsorption took place at 90% RH, a sharp increase in deflection was clearly seen at the beginning of the 90% RH period in CLT beams 1 and 2, followed by a slower increase rate. Overall, the increase in deflection at a high RH level was more significant than that at a low RH level.

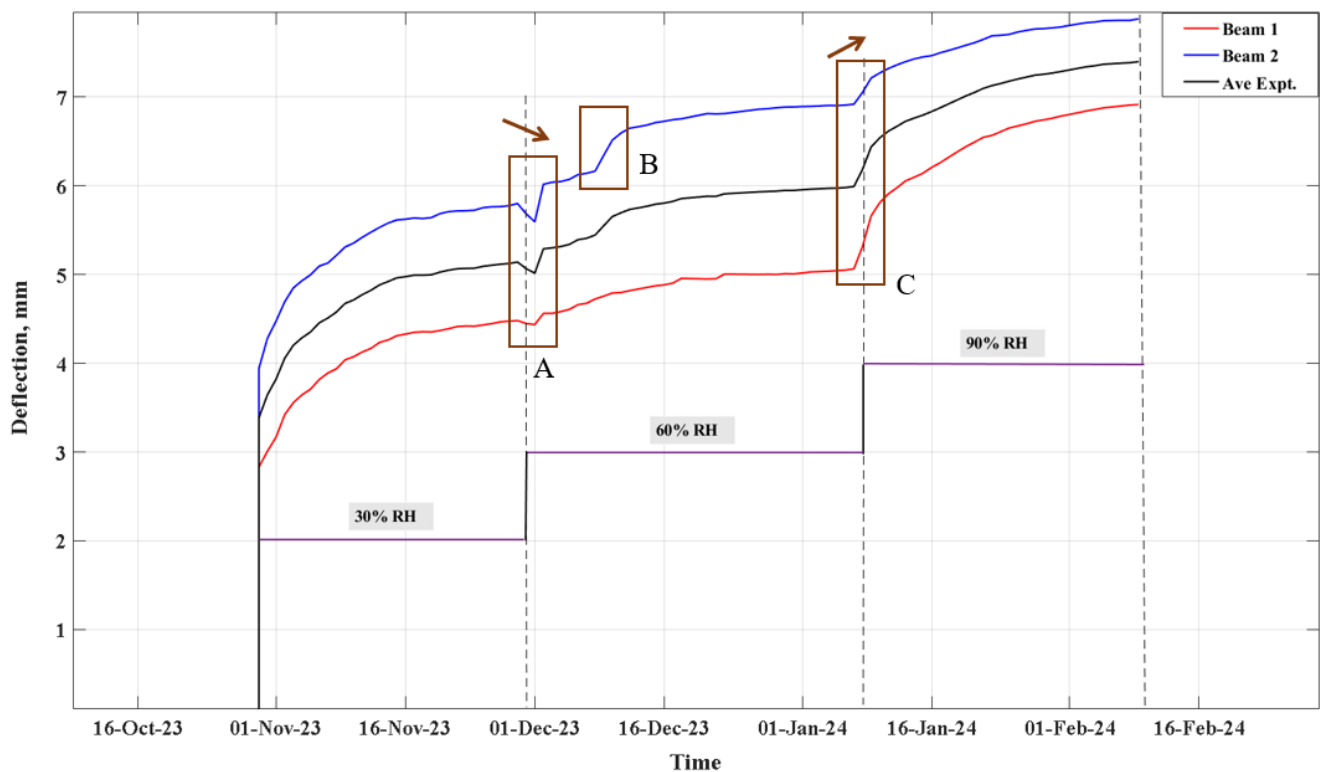


Figure 2. 10 Experimental creep deflection results of the CLT beams

## 2.4.2 Numerical Results

This section provides results summary and discussion for the moisture content distribution and creep deflection of the FE CLT beam. Since it is widely agreed that temperature has little influence on the expansion or contraction of the CLT beam, resulting strain and creep deflection are minimal. Hence, the temperature distribution is not reported and discussed further in this context.

### 2.4.2.1 Moisture Content Distribution in the FE Model

Figures 2.11, 2.12, and 2.13 show the predicted moisture content distribution of the CLT beam (full model and half section) at the end of the 30%, 60%, and 90% RH, respectively. The initial moisture content was assumed to be 12% because the CLT beams were conditioned at  $23 \pm 2^\circ\text{C}$  and  $53 \pm 5\%$  RH in the environmental chamber. As expected, the moisture content of the CLT beam did decrease to about 6% at the end of the 30% RH testing period because of moisture desorption. Then, due to moisture adsorption, it did increase to about 11% and 20% at the end of the testing period of 60% and 90% RH, respectively. The simulated moisture content values of the CLT beam at three RH levels aligned with the EMC readings from the EMC curve of spruce wood measured using DVS at  $25^\circ\text{C}$ . From the moisture content distribution in the middle lamina of CLT beam, i.e., the core of the CLT beam, at three RH levels, a relatively uniform moisture distribution was observed. It means that the one-month conditioning time is long enough to allow the whole piece of CLT beam to reach an equilibrium status.

Figure 2.14 shows plots of the FE CLT beam MC from three different locations, edge, core of the mid span, and top surface of mid span. During the 30% RH, the MC reading from the edge of the FE CLT decreased rapidly to about 6%, and then increased rapidly to about 11% and 20% during the 60% and 90% RH, respectively. The edges lose and gain MC rapidly compared to other locations and the numerical model can predict the MC of the CLT accurately. For the other locations, as expected the core of the CLT loses and gains MC gradually compared to the top

surface or/and edge. In general, the FE model predicted the moisture content well. The experiment could be improved by revising the setup to place paired CLT beams for moisture content check at different locations using a moisture meter over a three-month period to validate the transient moisture diffusion model further.

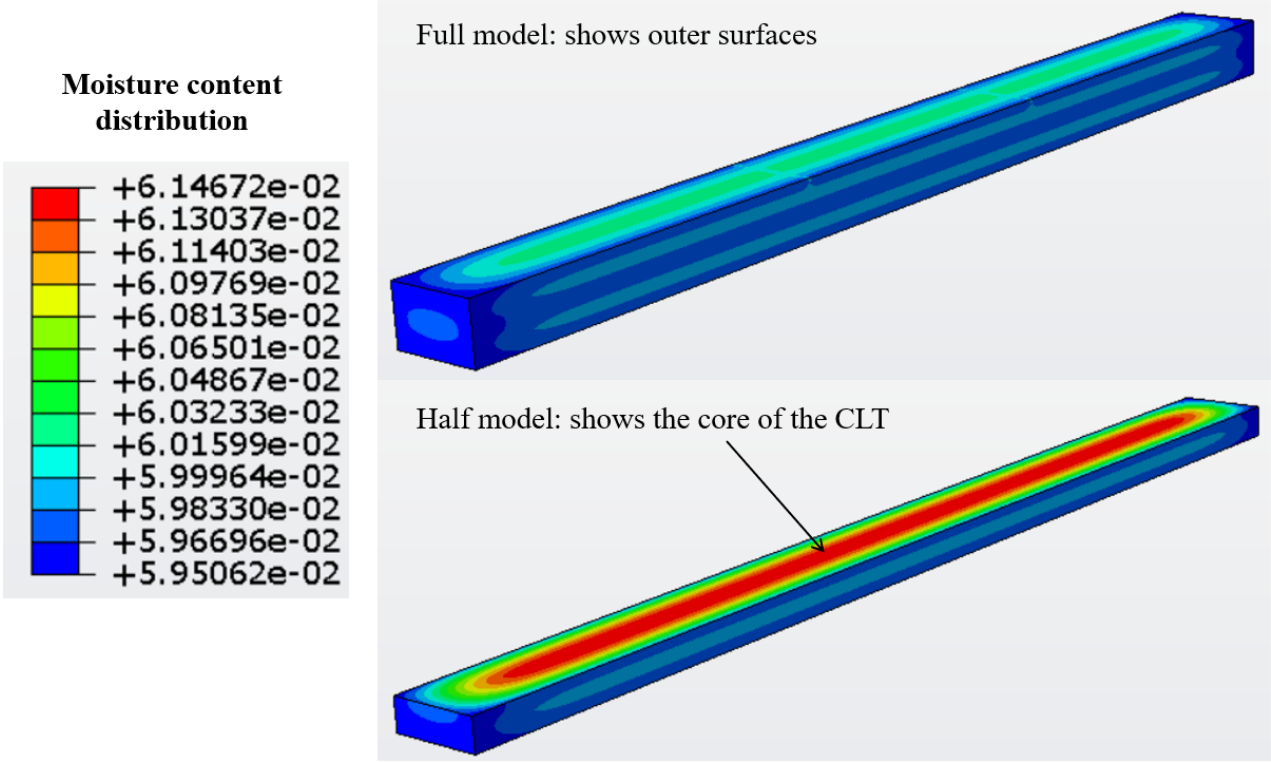


Figure 2. 11 Moisture content distribution of the FE CLT after the 30% RH testing period

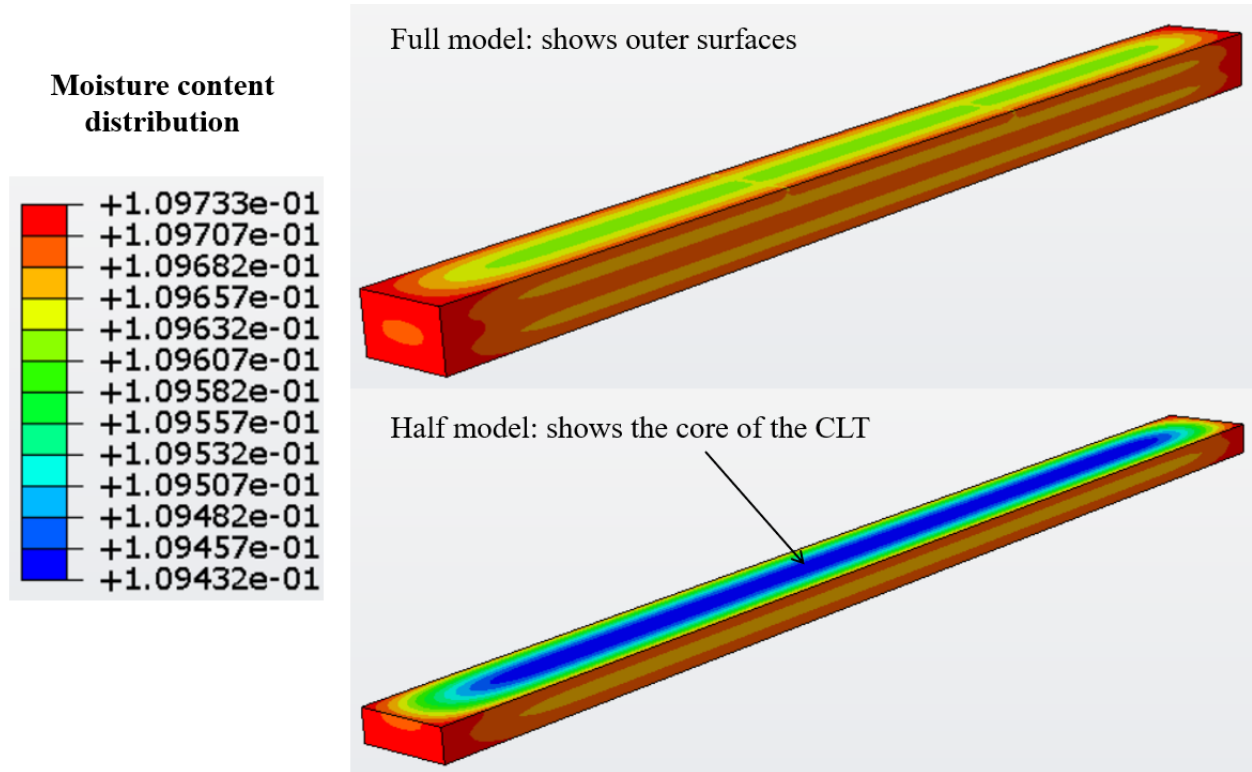


Figure 2. 12 Moisture content distribution of the FE CLT after the 60% RH testing period

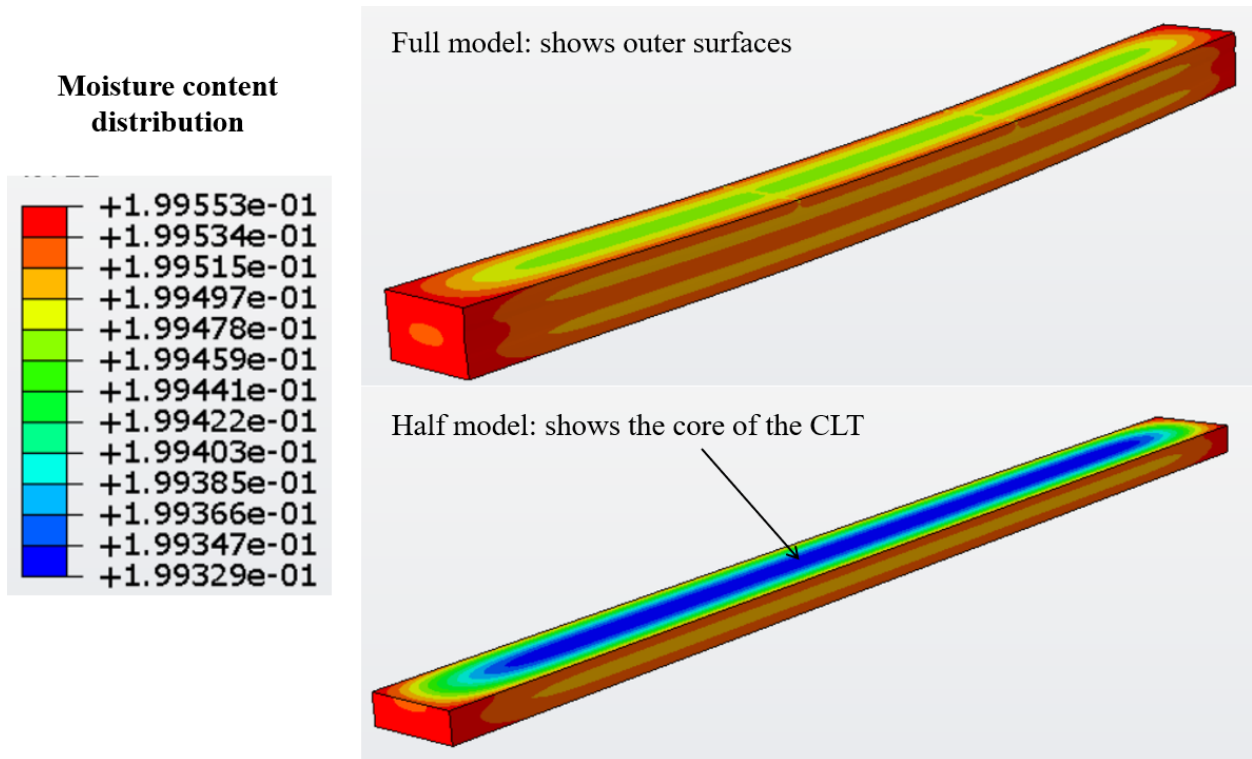


Figure 2. 13 Moisture content distribution of the FE CLT after the 90% RH testing period

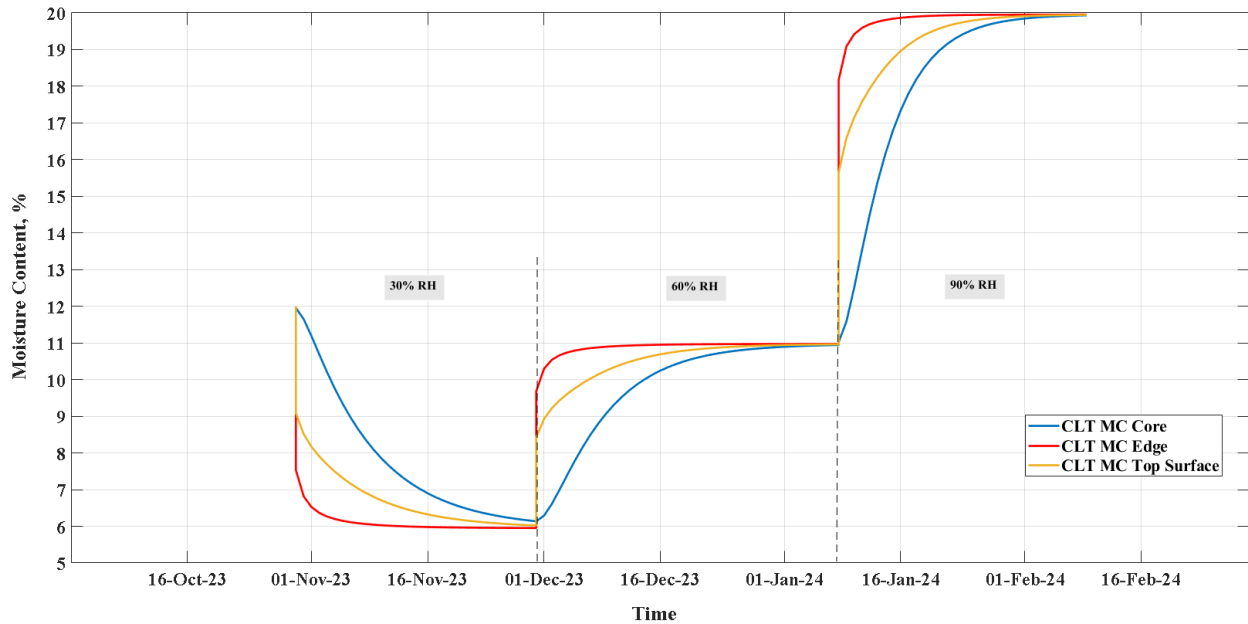


Figure 2. 14 Plot of moisture content of the FE CLT model from three different locations

#### 2.4.2.2 Creep Deflection of the FE Model

The creep deflection of the CLT beam obtained from the numerical model is plotted and compared with experiment as shown in Figure 2.15. Overall, the simulated results (red, solid line) agreed well with the average experimental data (black, solid line). Table 2.2 lists the elastic deflection, creep deflection results at the end period of 30% RH, 60% RH, and 90% RH, as well as the difference between experimental and simulated results. The FE model predicted the initial elastic deflection well with an experimental mean initial deflection of 3.38 mm compared to the numerical model deflection of 3.06 mm. The difference between experimental and simulated results is about 9.9 %, which may be caused by the differential in MOE of the input value and real CLT specimens tested. Additionally, at the end period of three RH levels, the difference between the deflection of experimental and simulated results was about 2.9 %, 2.7 %, and 4.4 %, respectively. In general, the total simulated long-term deflection of the CLT beam is in good correlation with the average experimental result. Even though the FE model used the material parameters obtained from published data, it is great to see the parameters including moisture diffusion coefficients, surface emission coefficient, moisture induced expansion and shrinkage coefficients, and coefficients of

mechano-sorptive compliance matrix could be used to simulate the creep evolution of spruce wood under RH fluctuations.

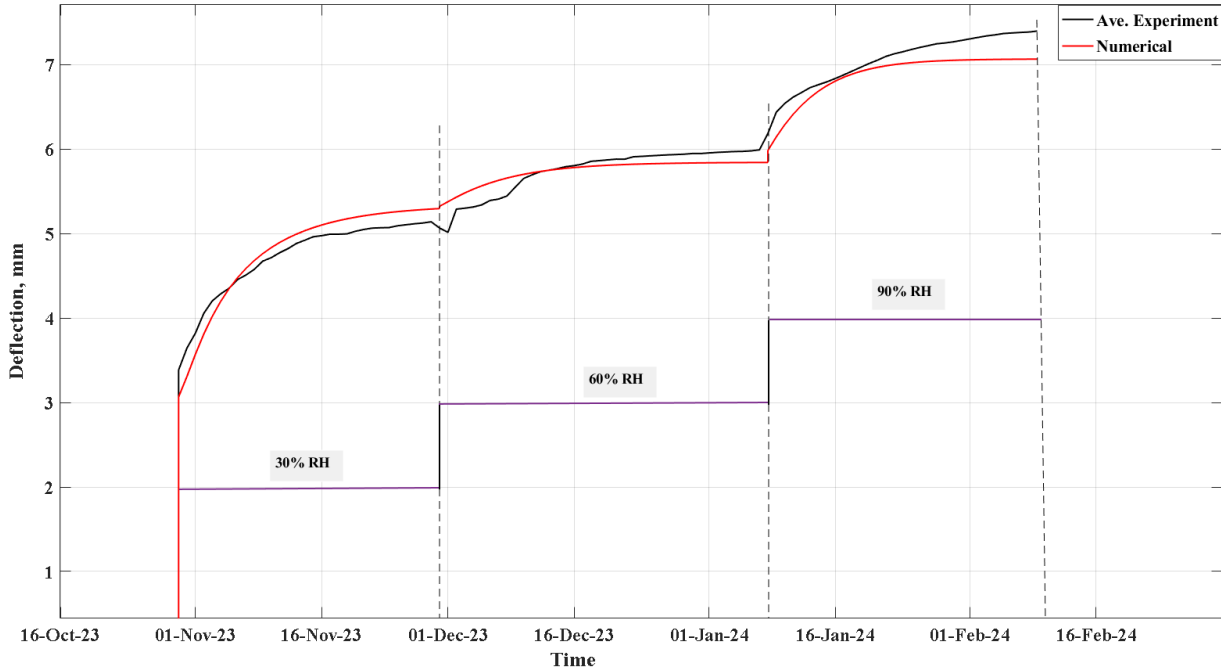


Figure 2. 15 The numerical creep deflection of the CLT beam compared to the mean experimental result

Table 2. 2 Comparison between the experimental and numerical deflection

<b>Deflection Extracted</b>	<b>Experiment (mm)</b>	<b>FE Model (mm)</b>	<b>Percentage Difference (%)</b>
Elastic phase	3.38	3.06	9.94
End period of 30% RH	5.14	5.29	2.88
End period of 60% RH	6.00	5.84	2.70
End period of 90% RH	7.39	7.07	4.43

## 2.5 Conclusion

The creep behavior of CLT beams were investigated using numerical simulations and validated with experimental data. The CLT beam was loaded simultaneously with constant dead load and elevated three levels of relative humidities, 30%, 60%, and 90%. The FE model predicted the MC distribution of the CLT very well. The MC of the FE CLT beam decreased to about 6% at the end of the 30% RH testing period. Then, it did increase to about 10.9% and 19.9% due to moisture adsorption at the end of the testing period of 60% and 90% RH, respectively. The predicted MC values of the CLT beam aligned well with the readings from the EMC curve of spruce wood measured using DVS at 25°C. Furthermore, the numerical creep deflection of the CLT beam correlated well with experiment, as indicated by the simulated results closely matching the experimental results at four checkpoints, with a difference of less than 10%. It should be noted that the computational model excluded the viscoelastic creep or creep strain from evaluating the total strain, and still the FE model gave good prediction of the creep behavior of CLT beam. This supports the fact that the mechano-sorptive strain was dominated. In general, the FE results correlated well with experimental data by utilizing a combination of experimental measurements (MOE in the longitudinal direction) and published data on materials.

One important improvement to the current FE model could take into consideration the difference in moisture diffusion coefficient during the adsorption phase and desorption phase by establishing an empirical equation using DVS experimental data . Also, to incorporate the viscoelastic strain, the proper properties or constants of the tested material must be defined to predict the viscoelastic creep well. These improvements would help to simulate the creep behavior more accurately. In addition to the FE model improvements, a sensitivity analysis can be performed using the FE creep model to determine the influence of each strain component on the creep behavior.

## References

### CHAPTER 1:

- [1] CLT handbook: cross-laminated timber, 2013.
- [2] S. Meulmann and E. Latifi, "Modelling and testing of CLT panels for evaluation of stiffness," Linnaeus University, Swedin, 2021.
- [3] A. Thiel and G. Schickhofer, "CLTdesigner - a software tool for designing cross laminated timber elements: 1D-plate-design," in *World conference on timber engineering*, Riva del Garda, Italy, 2010.
- [4] J. G. Ren, "A new theory of laminated plate," *Composite Science and Technology*, pp. 225-239, 1986.
- [5] D. R. Cook, D. S. Malkus and M. E. Plesha, *Concepts and Applications of Finite Element Analysis* (3rd Ed.), New York: John Wiley & Sons, 1989.
- [6] L. Franzoni, A. Lebee, F. Lyon and G. Foret, "Influence of orientation and number of layers on the elastic response and failure modes on CLT floors: modeling and parameter studies," *European Journal of Wood and Wood Products*, vol. 74, pp. 671-684, 2016.
- [7] L. Franzoni, A. Lebee, F. Lyon and G. Foret, "Elastic behavior of cross-laminated timber and timber panels with regular gaps: thick-plate modeling and experimental validation," *Engineering Structures*, vol. 141, pp. 402-416, 2017.
- [8] M. He, X. Sun and Z. Li, "Bending and compressive properties of cross-laminated timber (CLT) panels made from Canadian hemlock," *Construction and Building materials*, vol. 185, pp. 175-183, 2018.
- [9] Y. Chen and F. Lam, "Bending performance of box-based cross laminated timber systems," *Journal of Structural Engineering*, vol. 139, no. 12, 2012.
- [10] M. Gharib, A. Hassanieh, H. Valipour and M. Bradford, "Three-dimensional constitutive modelling of arbitrarily oriented timber based on continuum damage mechanics," *Finite Elements in Analysis and Design*, vol. 135, pp. 79-90, 2017.
- [11] B. Brank, A. Stanic, M. Lavrencic and B. Hudobivnik, "Design optimization and failure modelling of ribbed cross-laminated timber plates," in *Proceedings of the 11th International Conference "Shell Structures: Theory and Applications"*, Poland, 2017.

- [12] T. Gecys, A. Daniunas, T. K. Bader, L. Wagner and J. Eberhardsteiner, "3D finite element analysis and experimental investigations of a new type of timber beam-to-beam connection," *Engineering Structures*, vol. 12, pp. 134-145, 2015.
- [13] Y. Wang, J. Zhang, F. Mei, J. Liao and W. Li, "Experimental and numerical analysis on fire behaviour of loaded cross-laminated timber panels," *Advances in Structural Engineering*, vol. 23, pp. 22-36, 2020.
- [14] ABAQUS, "ABAQUS user's manual," Dassault Systemes Simulia Corp., 2021.
- [15] ASTM, "Standard test methods for small clear specimens of timber. ASTM D143-22," ASTM, Conshocken, PA, 2022.
- [16] ASTM, "Standard test methods of static tests of lumber in structural sizes. ASTM D198-22," ASTM, Conshocken, PA, 2022.
- [17] J. Bodig and B. A. Jayne, *Mechanics of wood and wood composites*, Reprint Edition ed., Krieger Publishing Company, 1993.
- [18] *Wood Handbook: wood as an engineering material*, vol. 190, USDA Forest Service, Forest Product Laboratory, General Technical Report FPL-GRT, 2010.
- [19] Z. Hashin, "Failure Criteria for Unidirectional Fiber Composites," *Journal of Applied Mechanics*, vol. 47, pp. 329-334, 1980.
- [20] K. Warren, R. Lopez-Anido, S. Vel and H. Bayraktar, "Progressive failure analysis of three-dimensional woven carbon composites in single-bolt, double-shear bearing," *Composites Part B*, vol. 84, pp. 266-276, 2016.
- [21] M. Alabbad, S. Vel and R. Lopez-Anido, "Computational model for predicting the low-velocity impact resistance and tolerance of composite laminates," *Composite Part B: Engineering*, vol. 244, 2022.
- [22] C. Sandhaas, A. K. Sarnaghi and J.-W. van de Kuilen, "Numerical modelling of timber and timber joints: computational aspects," *Wood Science and Technology*, vol. 54, pp. 31-61, 2020.
- [23] K. B. Dahl, "Mechanical properties of clear wood from Norway spruce," Norwegian University of Science and Technology, Trondheim, 2009.

- [24] S. A. Rahman, M. Ashraf and M. Subhani, "Comparison of continuum damage models for nonlinear finite element analysis of timber under tension in parallel and perpendicular to grain directions," *European Journal of Wood and Wood Products*, vol. 80, pp. 771-790, 2022.
- [25] E. J. Barbero, *Introduction to Composite Materials Design*, Taylor & Francis Group, 2011.
- [26] K. Santaoja, T. Leino, A. Ranta-Maunus and A. Hanhijarvi, "Mechano-sorption structural analysis of wood by the ABAQUS finite element program," *Technical Research Center of Finland, Espoo*, 1991.
- [27] F. Mirianon, S. Fortino and T. Toratti, "A method to model wood by using ABAQUS finite element software: part 1 constitutive model and computational details," *VTT Technical Research Center of Finland*, 2008.
- [28] "Element5 Mass Timber Manufacturer," [Online]. Available: <https://elementfive.co/>.

## **CHAPTER 2:**

- [1] J. Bodig and B. A. Jayne, *Mechanics of wood and wood composites*, Reprint Edition ed., Krieger Publishing Company, 1993.
- [2] C. Dong, S. Zhang, J. Wang and Y. H. Chui, "Static bending creep properties of furfurylated poplar wood," *Construction and Building Materials*, vol. 269, 2021.
- [3] J. Senft and S. Suddarth, "An analysis of creep-inducing stress in Sitka spruce," *Wood and Fiber Science*, vol. 2, pp. 321-327, 1971.
- [4] T. Toratti, "Creep of Timber Beams in a Variable Environment," *Laboratory of Structural Engineering and Building Physics*, Helsinki University of Technology, Espoo, 1992.
- [5] R. W. Davidson, "The influence of temperature on creep in wood," *Forest Product Journal*, vol. 12, pp. 377-381, 1962.
- [6] S. Hering and P. Niemz, "Moisture-dependent, viscoelastic creep of European beech wood in longitudinal direction," *European Journal of Wood and Wood Products*, vol. 70, pp. 667-670, 2012.

- [7] T. T. Nguyen, T. N. Dao, S. Aaleti, K. Hossain and K. Fridley, "Numerical Model for Creep Behavior of Axially Loaded CLT Panels," *Journal of Structural Engineering*, vol. 145, no. 1, 2018.
- [8] N. Yazdani, E. Johnson and S. Duwadi, "Creep effect in structural composite lumber for bridge applications," *Journal of Bridge Engineering*, vol. 9, no. 1, pp. 87-94, 2003.
- [9] J. C. Simo and T. J. R. Hughes, "Computational Inelasticity," *Springer-Verlag*, 1998.
- [10] C. O'Ceallaigh, K. Sikora, D. McPolin and A. M. Harte, "Modelling the hygro-mechanical creep behaviour of FRP reinforced timber elements," *Construction and Building Materials*, vol. 259, 2020.
- [11] L. Armstrong and G. Christensen, "Influence of Moisture Changes on Deformation of Wood Under Stress," *Nature*, vol. 191, pp. 869-870, 1961.
- [12] E. Gibson, "Creep of Wood: Role of Water and Effect of a Changing Moisture Content," *Nature*, vol. 206, pp. 213-215, 1965.
- [13] S. Mohager and T. Toratti, "Long term bending creep of wood in cyclic relative humidity," *Wood Science and Technology*, vol. 27, pp. 49-59, 1992.
- [14] Y. Huang, "Creep behavior of wood under cyclic moisture changes: interaction between load effect and moisture effect," *Journal of Wood Science*, vol. 62, pp. 392-399, 2016.
- [15] K. Santaoja, T. Leino, A. Ranta-Maunus and A. Hanhijärvi, "Mechano-sorption structural analysis of wood by the ABAQUS finite element program," Technical Research Centre of Finland, Espoo, 1991.
- [16] CLT handbook: cross-laminated timber, 2013.
- [17] ABAQUS, "ABAQUS user's manual," Dassault Systemes Simulia Corp., 2021.
- [18] A. V. Luikov, "Systems of differential equations of heat and mass transfer in capillary-porous bodies (review)," *International Journal of Heat and Mass Transfer*, vol. 18, no. 1, pp. 1-14, 1975.
- [19] H. Z. Zhou, E. C. Zhu, S. Fortino and T. Toratti, "Modelling the hygrothermal stress in curved glulam beams," *The Journal of Strain Analysis for Engineering Design*, vol. 45, no. 2, pp. 129-140, 2010.

- [20] S. Fortino, F. Mirianon and T. Toratti, "3D moisture-stress FEM analysis for time dependent problems in timber structures," *Mech Time-Depend Mater*, vol. 13, pp. 333-356, 2009.
- [21] A. Hanhijärvi, "Modelling of Creep Deformation Mechanisms in Wood," Technical Research Center of Finland, Espoo, Finland, 1995.
- [22] P. Becker, "Modellierung des zeit- und feuchteabhängigen Materialverhaltens zur Untersuchung des Langzeitverhaltens von Druckstäben aus Holz," Bauhaus-Universität Weimar, 2002.
- [23] A. Mårtensson, "Mechanical behaviour of wood exposed to humidity variations," 1992.
- [24] F. Mirianon, S. Fortino and T. Toratti, "A method to model wood by using ABAQUS finite element software: Part 1. Constitutive Model and Computational Details," VTT Technical Research Centre of Finland, Espoo, 2008.
- [25] S. Ormarsson, "Numerical analysis of moisture related distortions in sawn timber," Chalmers University of Technology, Sweden, 1999.
- [26] J. Kangas and A. Ranta-Maunus, "Creep tests on the Finnish pine and spruce perpendicular to the grain Research Notes 969," Technical Research Centre of Finland, Espoo, 1989.
- [27] N. E. Dowling, *Mechanical Behavior of Materials* (4<sup>th</sup> edition), Person, 2013.

## **BIOGRAPHY OF THE AUTHOR**

Maitham Alabbad was born in Saudi Arabia. He received his B.S. degree in Mechanical Engineering from the University of Maine in 2017. He continued to obtain a Master of Science degree in Mechanical Engineering from the University of Maine in 2020. Maitham worked as a graduate research assistant in the field of solid mechanics, and as a graduate teaching assistant for the Department of Mechanical Engineering. Maitham Alabbad is a candidate for the Master of Science degree in Forest Resource with concentration in Bioproducts Engineering at the University of Maine in August 2024.